Journal of Scientific Computing manuscript No.
(will be inserted by the editor)

Stabilized Finite Element Methods for the Oberbeck-Boussinesq Model

Helene Dallmann · Daniel Arndt

August 26, 2015

Abstract We consider conforming finite element (FE) approximations for the time-dependent Oberbeck-Boussinesq model with inf-sup stable pairs for velocity and pressure and use a stabilization of the incompressibility constraint. In case of dominant convection, a local projection stabilization (LPS) method in streamline direction is considered both for velocity and temperature. For the arising nonlinear semi-discrete problem, a stability and convergence analysis is given that does not rely on a mesh width restriction. Numerical experiments validate a suitable parameter choice within the bounds of the theoretical results.

Keywords Oberbeck-Boussinesq model; Navier-Stokes equations; stabilized finite elements; local projection stabilization; grad-div stabilization; non-isothermal flow

Mathematics Subject Classification (2000) MSC 65M12 · MSC 65M60 · MSC 76D05

1 Introduction

In this paper, we consider non-isothermal incompressible flow using the Oberbeck-Boussinesq approximation [1,2]. This model is applicable if only small temperature differences occur and hence, the density is constant. The equations read:

$$\begin{aligned} \partial_t \boldsymbol{u} - \nu \Delta \boldsymbol{u} + (\boldsymbol{u} \cdot \nabla)\boldsymbol{u} + \nabla p + \beta\theta \boldsymbol{g} &= \boldsymbol{f}_u \quad \text{in } (0,T)\times\Omega, \\ \nabla \cdot \boldsymbol{u} &= 0 \quad \text{in } (0,T)\times\Omega, \\ \partial_t \theta - \alpha \Delta \theta + (\boldsymbol{u} \cdot \nabla)\theta &= f_\theta \quad \text{in } (0,T)\times\Omega \end{aligned} \tag{1}$$

The first author was supported by the RTG 1023 founded by German research council (DFG).
The second author was supported by CRC 963 founded by German research council (DFG).

Institute of Numerical and Applied Mathematics,
Georg-August University of Göttingen, D-37083, Germany
Tel.: +49-551-394531
Fax: +49-551-3933944
E-mail: h.dallmann/d.arndt@math.uni-goettingen.de

together with initial and boundary conditions in a domain $\Omega \subset \mathbb{R}^d$, $d \in \{2, 3\}$, with boundary $\partial\Omega$. Here $\boldsymbol{u}\colon [0,T] \times \Omega \to \mathbb{R}^d$, $p\colon [0,T] \times \Omega \to \mathbb{R}$ and $\theta\colon [0,T] \times \Omega \to \mathbb{R}$ denote the unknown velocity, pressure and temperature fields for given viscosity $\nu > 0$, thermal diffusivity $\alpha > 0$, thermal expansion coefficient $\beta > 0$, external forces $\boldsymbol{f}_u$, f_θ, gravitation $\boldsymbol{g}$.

Discretizations using finite element methods (FEM) often suffer from spurious oscillations in the numerical solution that arise for example due to dominating convection, internal shear or near boundary layers or poor mass conservation.

The so-called grad-div stabilization is an additional element-wise stabilization of the divergence constraint. It enhances the discrete mass conservation and reduces the effect of the pressure error on the velocity error (cf. [3,4]). It plays an important role for robustness.

Local projection based stabilization (LPS) methods rely on the idea to separate the discrete function spaces into small resolved and large resolved scales and to add stabilization terms only on the small scales. In [5], LPS methods are analyzed for the stationary Oseen problem, where an additional compatibility condition between the approximation and projection velocity ansatz spaces is assumed. Thus, stability and error bounds of optimal order can be established. Furthermore, suitable simplicial and quadrilateral ansatz spaces are suggested that fulfill the compatibility condition. In the paper [6], the authors provide an overview regarding stabilized finite element methods for the Oseen problem, in particular for local projection stabilization methods using inf-sup stable pairs. The unified representation gives an overview over suitable ansatz spaces including parameter design.

In [7] and [8], conforming finite element approximations of the time-dependent Oseen and Navier-Stokes problems with inf-sup stable approximation of velocity and pressure are considered. For handling the case of high Reynolds numbers, local projection with streamline upwinding (LPS SU) and grad-div stabilizations are applied and stability and convergence are shown. For general LPS variants, a local restriction of the mesh width is required to obtain methods of (quasi-)optimal order; this can be circumvented by using the compatibility condition from [5]. The positive effect of additional element-wise stabilization of the divergence constraint becomes apparent in the analysis as well as in the numerical experiments. Recent results from [9] for the time-dependent Oseen problem reinforce the benefits and stabilizing effects of grad-div stabilization for inf-sup stable mixed finite elements. The authors show that the Galerkin approximations can be stabilized by adding only grad-div stabilization.

Early numerical analysis for thermally coupled flow can be found in [10,11, 12]. In [13,14], subgrid-scale modeling for turbulent temperature dependent flow is considered. Since local projection and grad-div stabilization have proven useful for a large range of critical parameters, we want to apply them to the Oberbeck-Boussinesq model (1) and assess their performance.

This paper is structured as follows:

In Section 2, we introduce a finite element semi-discretization for the Oberbeck-Boussinesq model with grad-div and LPS SU stabilization and prove stability in Section 3.

We extend the convergence analysis without compatibility condition from [7] for the Oseen problem and [8] for the Navier-Stokes equations to the thermally

coupled setting in Section 4. Here, we can circumvent a restriction of the mesh width. The estimates rely on the discrete inf-sup stability of the velocity and pressure ansatz spaces and the existence of a local interpolation operator preserving the divergence as well as on relatively mild regularity assumptions for the continuous solutions. The convective terms are treated carefully in order to circumvent an exponential deterioration of the error in the limit of vanishing diffusion. Furthermore, a pressure estimate is given using the discrete inf-sup stability. The applicability of the proposed methods to possible finite element settings is discussed and the design of stabilization parameters is studied.

The subsequent Section 5 is devoted to the numerical simulation of incompressible non-isothermal flow. First, we present the time-discretization of the model and state some analytical results. We use a method called pressure-correction projection method, which incorporates a backward differentiation formula of second order. We validate the theoretical convergence results with respect to the mesh width and study the influence of grad-div and LPS stabilization on the errors for the parameter range suggested by the analysis. As a more realistic flow, Rayleigh-Bénard convection is considered. The stabilization variants are applied and their performance evaluated via suitable benchmarks.

2 The Discretized Oberbeck-Boussinesq Problem

In this section, we describe the model problem and the spatial semi-discretization based on inf-sup stable interpolation of velocity and pressure together with grad-div and local projection stabilization of the velocity and temperature gradients in streamline direction.

2.1 The Oberbeck-Boussinesq model

Let $\Omega \subset \mathbb{R}^d$, $d \in \{2, 3\}$, be a bounded polyhedral Lipschitz domain with boundary $\partial\Omega$. For simplicity, we consider homogeneous Dirichlet boundary conditions for velocity and temperature.

In the following, we consider Sobolev spaces $W^{m,p}(\Omega)$ with norm $\|\cdot\|_{W^{m,p}(\Omega)}, m \in \mathbb{N}_0, p \geq 1$. In particular, we have $L^p(\Omega) = W^{0,p}(\Omega)$. For $K \subseteq \Omega$, we will write

$$\|u\|_0 := \|u\|_{L^2(\Omega)}, \qquad \|u\|_{0,K} := \|u\|_{L^2(K)},$$
$$\|u\|_\infty := \|u\|_{L^\infty(\Omega)}, \qquad \|u\|_{\infty,K} := \|u\|_{L^\infty(K)}.$$

Moreover, the closed subspaces $W_0^{1,2}(\Omega)$, consisting of functions in $W^{1,2}(\Omega)$ with zero trace on $\partial\Omega$, and $L_0^2(\Omega)$, consisting of L^2-functions with zero mean in Ω, will be used. The inner product in $L^2(K)$ will be denoted by $(\cdot,\cdot)_K$. In case of $K = \Omega$, we omit the index. With this, we define suitable function spaces:

$$\boldsymbol{V} := [W_0^{1,2}(\Omega)]^d, \qquad Q := L_0^2(\Omega), \qquad \Theta := W_0^{1,2}(\Omega).$$

The variational formulation of (1) for fixed time $t \in (0, T)$ reads:

Find $(\boldsymbol{u}(t), p(t), \theta(t)) \in \boldsymbol{V} \times Q \times \Theta$ such that it holds for all $(\boldsymbol{v}, q, \psi) \in \boldsymbol{V} \times Q \times \Theta$

$$\begin{aligned}(\partial_t \boldsymbol{u}(t), \boldsymbol{v}) + (\nu \nabla \boldsymbol{u}(t), \nabla \boldsymbol{v}) + c_u(\boldsymbol{u}(t); \boldsymbol{u}(t), \boldsymbol{v}) \\ -(p(t), \nabla \cdot \boldsymbol{v}) + (\beta \theta(t) \boldsymbol{g}, \boldsymbol{v}) = (\boldsymbol{f}_u(t), \boldsymbol{v}), \qquad (2) \\ (\nabla \cdot \boldsymbol{u}(t), q) = 0, \\ (\partial_t \theta(t), \psi) + (\alpha \nabla \theta(t), \nabla \psi) + c_\theta(\boldsymbol{u}(t); \theta(t), \psi) = (f_\theta(t), \psi) \qquad (3)\end{aligned}$$

with

$$\begin{aligned}c_u(\boldsymbol{w}; \boldsymbol{u}, \boldsymbol{v}) &:= \frac{1}{2}\big[((\boldsymbol{w} \cdot \nabla)\boldsymbol{u}, \boldsymbol{v}) - ((\boldsymbol{w} \cdot \nabla)\boldsymbol{v}, \boldsymbol{u})\big], \\ c_\theta(\boldsymbol{w}; \theta, \psi) &:= \frac{1}{2}\big[((\boldsymbol{w} \cdot \nabla)\theta, \psi) - ((\boldsymbol{w} \cdot \nabla)\psi, \theta)\big].\end{aligned}$$

The skew-symmetric forms of the convective term c_u and c_θ are chosen for conservation purposes. The forces are required to satisfy $\boldsymbol{f}_u \in L^2(0,T;[L^2(\Omega)]^d) \cap C(0,T;[L^2(\Omega)]^d)$, $f_\theta \in L^2(0,T;L^2(\Omega)) \cap C(0,T;L^2(\Omega))$ and $\boldsymbol{g} \in L^\infty(0,T;[L^\infty(\Omega)]^d)$ and the initial data is assumed to fulfill $\boldsymbol{u}_0 \in [L^2(\Omega)]^d$, $\theta_0 \in L^2(\Omega)$. In this paper, we will additionally assume that $\boldsymbol{u} \in L^\infty(0,T;[W^{1,\infty}(\Omega)]^d)$ and $\theta \in L^\infty(0,T;W^{1,\infty}(\Omega))$ which ensures uniqueness of the solution.

2.2 The Stabilized Semi-Discrete Model

For the discretization in space, finite element methods are applied. For the Galerkin formulation of (2)-(3), we approximate the solution spaces $\boldsymbol{V}$, Q, Θ by finite dimensional conforming subspaces $\boldsymbol{V}_h \subset \boldsymbol{V}$, $Q_h \subset Q$, $\Theta_h \subset \Theta$. We impose a discrete inf-sup condition for $\boldsymbol{V}_h$ and Q_h throughout this paper: Let $\boldsymbol{V}_h \subset \boldsymbol{V}$ and $Q_h \subset Q$ be FE spaces satisfying a discrete inf-sup-condition

$$\inf_{q_h \in Q_h \setminus \{0\}} \sup_{\boldsymbol{v}_h \in \boldsymbol{V}_h \setminus \{\boldsymbol{0}\}} \frac{(\nabla \cdot \boldsymbol{v}_h, q_h)}{\|\nabla \boldsymbol{v}_h\|_0 \|q_h\|_0} \geq \beta_d > 0 \qquad (4)$$

with a constant β_d independent of h.

In particular, due to the closed range theorem, the set of weakly solenoidal functions

$$\boldsymbol{V}_h^{div} := \{\boldsymbol{v}_h \in \boldsymbol{V}_h \mid (q_h, \nabla \cdot \boldsymbol{v}_h) = 0 \ \forall\ q_h \in Q_h\} \qquad (5)$$

does not only consist of the zero-function.

The semi-discrete Galerkin solution of problem (2)-(3) may suffer from spurious oscillations due to poor mass conservation and/or dominating advection. The idea of local projection stabilization (LPS) methods is to separate discrete function spaces into small and large scales and to add stabilization terms only on small scales. The grad-div stabilization is an additional element-wise stabilization of the divergence constraint and enhances the discrete mass conservation.

Let $\{\mathcal{T}_h\}$, $\{\mathcal{M}_h\}$, $\{\mathcal{L}_h\}$ be admissible and shape-regular families of non-overlapping triangulations. $\{\mathcal{M}_h\}$ and $\{\mathcal{L}_h\}$ denote macro decompositions of Ω for velocity and temperature, which represent the coarse scales in velocity and temperature. In the two-level approach, the large scales are defined by using a coarse mesh. The coarse mesh $\mathcal{M}_h$ is constructed such that each macro-element

$M \in \mathcal{M}_h$ is the union of one or more neighboring elements $T \in \mathcal{T}_h$. In the one-level LPS-approach, the coarse scales can be represented via a lower order finite elements space on $\mathcal{T}_h$. Another way is to enrich the fine spaces. We can use the same abstract framework by setting $\mathcal{M}_h = \mathcal{T}_h$. $\mathcal{L}_h$ is constructed analogously for the temperature.

There is $n_{\mathcal{T}_h} < \infty$ such that all M and L are formed as a conjunction of at most $n_{\mathcal{T}_h}$ cells $T \in \mathcal{T}_h$. Denote by h_T, h_M and h_L the diameters of cells $T \in \mathcal{T}_h$, $M \in \mathcal{M}_h$ and $L \in \mathcal{L}_h$, respectively. In addition, we require that there are constants C_1, $C_2 > 0$ such that

$$h_T \leq h_M \leq C_1 h_T, \quad h_T \leq h_L \leq C_2 h_T \quad \forall\, T \subset M,\ T \subset L,\ M \in \mathcal{M}_h,\ L \in \mathcal{L}_h.$$

We denote by $Y_h^u, Y_h^\theta \subset H^1(\Omega) \cap L^\infty(\Omega)$ finite element spaces of functions that are continuous on $\mathcal{T}_h$. We consider the conforming finite element spaces

$$\boldsymbol{V}_h = [Y_h^u]^d \cap \boldsymbol{V}, \qquad Q_h \subset Y_h^p \cap Q, \qquad \Theta_h = Y_h^\theta \cap \Theta$$

for velocity, pressure and temperature, where Y_h^p is a finite element space of functions on $\mathcal{T}_h$. Moreover, let $\boldsymbol{D}^u_{\mathcal{M}_h} \subset [L^\infty(\Omega)]^d$, $D^\theta_{\mathcal{L}_h} \subset L^\infty(\Omega)$ denote discontinuous finite element spaces on $\mathcal{M}_h$ for $\boldsymbol{u}_h$ and on $\mathcal{L}_h$ for θ_h, respectively. We set

$$\boldsymbol{D}^u_M = \{\boldsymbol{v}_h|_M \colon\ \boldsymbol{v}_h \in \boldsymbol{D}^u_{\mathcal{M}_h}\}, \qquad D^\theta_L = \{\psi_h|_L \colon\ \psi_h \in D^\theta_{\mathcal{L}_h}\}.$$

Later, we will write for combinations of finite element spaces

$$(\boldsymbol{V}_h / \boldsymbol{D}^u_M) \wedge Q_h \wedge (\Theta_h / D^\theta_L).$$

If no LPS is applied, we omit the respective coarse space in the above notation. For $M \in \mathcal{M}_h$ and $L \in \mathcal{L}_h$, let $\pi^u_M \colon [L^2(M)]^d \to \boldsymbol{D}^u_M$, $\pi^\theta_L \colon L^2(L) \to D^\theta_L$ be the orthogonal L^2-projections onto the respective macro spaces. The so-called fluctuation operators are defined by

$$\begin{aligned} &\kappa^u_M \colon [L^2(M)]^d \to [L^2(M)]^d, && \kappa^\theta_L \colon L^2(L) \to L^2(L), \\ &\kappa^u_M := Id - \pi^u_M, && \kappa^\theta_L := Id - \pi^\theta_L. \end{aligned}$$

For all macro elements $M \in \mathcal{M}_h$ and $L \in \mathcal{L}_h$, we denote the element-wise constant streamline directions of $\boldsymbol{u}_h \in \boldsymbol{V}_h$ by $\boldsymbol{u}_M \in \mathbb{R}^d$ and $\boldsymbol{u}_L \in \mathbb{R}^d$. One possible definition is

$$\boldsymbol{u}_M := \frac{1}{|M|} \int_M \boldsymbol{u}_h(\boldsymbol{x})\ \mathrm{d}\boldsymbol{x}, \qquad \boldsymbol{u}_L := \frac{1}{|L|} \int_L \boldsymbol{u}_h(\boldsymbol{x})\ \mathrm{d}\boldsymbol{x}. \tag{6}$$

With the introduced notation, we can define the spatially discretized Oberbeck-Boussinesq model with grad-div and LPS SU stabilization:

Find $(\boldsymbol{u}_h, p_h, \theta_h)\colon (0,T) \to \boldsymbol{V}_h \times Q_h \times \Theta_h$ such that for all $(\boldsymbol{v}_h, q_h, \psi_h) \in \boldsymbol{V}_h \times Q_h \times \Theta_h$:

$$\begin{aligned}(\partial_t \boldsymbol{u}_h, \boldsymbol{v}_h) + (\nu \nabla \boldsymbol{u}_h, \nabla \boldsymbol{v}_h) + c_u(\boldsymbol{u}_h; \boldsymbol{u}_h, \boldsymbol{v}_h) - (p_h, \nabla \cdot \boldsymbol{v}_h) + (\nabla \cdot \boldsymbol{u}_h, q_h) \\ + (\beta \boldsymbol{g} \theta_h, \boldsymbol{v}_h) + s_u(\boldsymbol{u}_h; \boldsymbol{u}_h, \boldsymbol{v}_h) + t_h(\boldsymbol{u}_h; \boldsymbol{u}_h, \boldsymbol{v}_h) = (\boldsymbol{f}_u, \boldsymbol{v}_h), \quad (7)\\ (\partial_t \theta_h, \psi_h) + (\alpha \nabla \theta_h, \nabla \psi_h) + c_\theta(\boldsymbol{u}_h; \theta_h, \psi_h) + s_\theta(\boldsymbol{u}_h; \theta_h, \psi_h) = (f_\theta, \psi_h) \quad (8)\end{aligned}$$

with the streamline-upwind (SUPG)-type stabilizations s_u, s_θ and the grad-div stabilization t_h according to

$$\begin{aligned}s_u(\boldsymbol{w}_h; \boldsymbol{u}, \boldsymbol{v}) &:= \sum_{M \in \mathcal{M}_h} \tau_M^u(\boldsymbol{w}_M)(\kappa_M^u((\boldsymbol{w}_M \cdot \nabla)\boldsymbol{u}), \kappa_M^u((\boldsymbol{w}_M \cdot \nabla)\boldsymbol{v}))_M,\\ s_\theta(\boldsymbol{w}_h; \theta, \psi) &:= \sum_{L \in \mathcal{L}_h} \tau_L^\theta(\boldsymbol{w}_L)(\kappa_L^\theta((\boldsymbol{w}_L \cdot \nabla)\theta), \kappa_L^\theta((\boldsymbol{w}_L \cdot \nabla)\psi))_L,\\ t_h(\boldsymbol{w}_h; \boldsymbol{u}, \boldsymbol{v}) &:= \sum_{M \in \mathcal{M}_h} \gamma_M(\boldsymbol{w}_M)(\nabla \cdot \boldsymbol{u}, \nabla \cdot \boldsymbol{v})_M\end{aligned}$$

and non-negative stabilization parameters τ_M^u, τ_L^θ, γ_M.

The set of stabilization parameters $\tau_M^u(\boldsymbol{u}_h)$, $\tau_L^\theta(\boldsymbol{u}_h)$, $\gamma_M(\boldsymbol{u}_h)$ has to be determined later on. Let the initial data be given as suitable interpolations of the continuous initial values in the respective finite element spaces as

$$\boldsymbol{u}_h(0) = j_u \boldsymbol{u}_0 =: \boldsymbol{u}_{h,0} \in \boldsymbol{V}_h \subset [L^2(\Omega)]^d, \quad \theta_h(0) = j_\theta \theta_0 =: \theta_{h,0} \in \Theta_h \subset L^2(\Omega),$$

where $(j_u, j_\theta)\colon \boldsymbol{V} \times \Theta \to \boldsymbol{V}_h \times \Theta_h$ denote interpolation operators. We remark that for solenoidal $\boldsymbol{u}_0$, we can find an interpolation operator j_u such that $\boldsymbol{u}_{h,0} \in \boldsymbol{V}_h^{div}$ (cf. [15]).

We point out that due to the discrete inf-sup condition, we can search for $(\boldsymbol{u}_h, p_h, \theta_h)\colon (0,T) \to \boldsymbol{V}_h^{div} \times Q_h \times \Theta_h$ in (7)-(8) equivalently.

3 Stability Analysis

We address the question regarding the existence of a semi-discrete solution of (7)-(8). This is obtained via a stability result for $\boldsymbol{u}_h \in \boldsymbol{V}_h^{div}$ and $\theta_h \in \Theta_h$; it yields control over the kinetic energy and dissipation. The definition of the mesh-dependent expressions below is motivated by symmetric testing in (7)-(8). For $\boldsymbol{v} \in \boldsymbol{V}$ and $\theta \in \Theta$, we define

$$\begin{aligned}|||\boldsymbol{v}|||_{LPS}^2 &:= \nu \|\nabla \boldsymbol{v}\|_0^2 + s_u(\boldsymbol{u}_h; \boldsymbol{v}, \boldsymbol{v}) + t_h(\boldsymbol{u}_h; \boldsymbol{v}, \boldsymbol{v}),\\ |[\theta]|_{LPS}^2 &:= \alpha \|\nabla \theta\|_0^2 + s_\theta(\boldsymbol{u}_h; \theta, \theta),\\ \|\boldsymbol{v}\|_{L^2(0,T;LPS)}^2 &:= \int_0^T |||\boldsymbol{v}(t)|||_{LPS}^2 \, \mathrm{d}t,\\ \|\theta\|_{L^2(0,T;LPS)}^2 &:= \int_0^T |[\theta(t)]|_{LPS}^2 \, \mathrm{d}t.\end{aligned}$$

The following result states the desired stability.

Theorem 1 *Assume $(\boldsymbol{u}_h, p_h, \theta_h) \in \boldsymbol{V}_h^{div} \times Q_h \times \Theta_h$ is a solution of (7)-(8) with initial data $\boldsymbol{u}_{h,0} \in [L^2(\Omega)]^d$, $\theta_{h,0} \in L^2(\Omega)$. For $0 \leq t \leq T$, we obtain*

$$\begin{aligned}
\|\theta_h\|_{L^\infty(0,t;L^2(\Omega))} &\leq \|\theta_{h,0}\|_0 + \|f_\theta\|_{L^1(0,T;L^2(\Omega))} =: C_\theta(T, \theta_{h,0}, f_\theta),\\
\|\boldsymbol{u}_h\|_{L^\infty(0,t;L^2(\Omega))} &\leq \|\boldsymbol{u}_{h,0}\|_0 + \|\boldsymbol{f}_u\|_{L^1(0,T;L^2(\Omega))}\\
&\quad + \beta\|\boldsymbol{g}\|_{L^1(0,T;L^\infty(\Omega))} \left(\|\theta_{h,0}\|_0 + \|f_\theta\|_{L^1(0,T;L^2(\Omega))}\right)\\
&=: C_u(T, \boldsymbol{u}_{h,0}, \theta_{h,0}, \boldsymbol{f}_u, f_\theta),\\
\|\theta_h\|_{L^2(0,t;LPS)} &\leq C_\theta(T, \theta_{h,0}, f_\theta),\\
\|\boldsymbol{u}_h\|_{L^2(0,t;LPS)} &\leq C_u(T, \boldsymbol{u}_{h,0}, \theta_{h,0}, \boldsymbol{f}_u, f_\theta).
\end{aligned}$$

Proof Let us start with the first claim for the temperature. Testing with $\psi_h = \theta_h \in \Theta_h$ in (8) gives

$$\frac{1}{2}\frac{d}{dt}\|\theta_h\|_0^2 + |[\theta_h]|_{LPS}^2 = (\partial_t\theta_h, \theta_h) + \alpha\|\nabla\theta_h\|^2 + s_\theta(\boldsymbol{u}_h; \theta_h, \theta_h) = (f_\theta, \theta_h). \tag{9}$$

Due to $s_\theta(\boldsymbol{u}_h; \theta_h, \theta_h) \geq 0$, it follows

$$\|\theta_h\|_0 \frac{d}{dt}\|\theta_h\|_0 = \frac{1}{2}\frac{d}{dt}\|\theta_h\|_0^2 \leq \|f_\theta\|_0\|\theta_h\|_0 \quad \Rightarrow \quad \frac{d}{dt}\|\theta_h\|_0 \leq \|f_\theta\|_0.$$

Integration in time leads to

$$\|\theta_h(t)\|_0 \leq \|\theta_{h,0}\|_0 + \|f_\theta\|_{L^1(0,T;L^2(\Omega))} = C_\theta(T, \theta_{h,0}, f_\theta). \tag{10}$$

For the velocity, we test with $(\boldsymbol{u}_h, 0) \in \boldsymbol{V}_h^{div} \times Q_h$ in (7)

$$\begin{aligned}
&\frac{1}{2}\frac{d}{dt}\|\boldsymbol{u}_h\|_0^2 + |||\boldsymbol{u}_h|||_{LPS}^2\\
&= (\partial_t\boldsymbol{u}_h, \boldsymbol{u}_h) + (\nu\nabla\boldsymbol{u}_h, \nabla\boldsymbol{u}_h) + s_u(\boldsymbol{u}_h; \boldsymbol{u}_h, \boldsymbol{u}_h) + t_h(\boldsymbol{u}_h; \boldsymbol{u}_h, \boldsymbol{u}_h)\\
&= (\boldsymbol{f}_u - \beta\boldsymbol{g}\theta_h, \boldsymbol{u}_h).
\end{aligned} \tag{11}$$

We obtain

$$\|\boldsymbol{u}_h\|_0 \frac{d}{dt}\|\boldsymbol{u}_h\|_0 = \frac{1}{2}\frac{d}{dt}\|\boldsymbol{u}_h\|_0^2 \leq \left(\|\boldsymbol{f}_u\|_0 + \beta\|\boldsymbol{g}\|_\infty\|\theta_h\|_0\right)\|\boldsymbol{u}_h\|_0.$$

Hence, $\frac{d}{dt}\|\boldsymbol{u}_h\|_0 \leq \|\boldsymbol{f}_u\|_0 + \beta\|\boldsymbol{g}\|_\infty\|\theta_h\|_0$. Integration in time and using stability of the temperature (10) give:

$$\begin{aligned}
\|\boldsymbol{u}_h(t)\|_0 &\leq \|\boldsymbol{u}_{h,0}\|_0 + \|\boldsymbol{f}_u\|_{L^1(0,t;L^2(\Omega))}\\
&\quad + \beta\|\boldsymbol{g}\|_{L^1(0,t;L^\infty(\Omega))}\|\theta_h\|_{L^\infty(0,t;L^2(\Omega))}\\
&\leq \|\boldsymbol{u}_{h,0}\|_0 + \|\boldsymbol{f}_u\|_{L^1(0,T;L^2(\Omega))}\\
&\quad + \beta\|\boldsymbol{g}\|_{L^1(0,T;L^\infty(\Omega))} \left(\|\theta_{h,0}\|_0 + \|f_\theta\|_{L^1(0,T;L^2(\Omega))}\right)\\
&= C_u(T, \boldsymbol{u}_{h,0}, \theta_{h,0}, \boldsymbol{f}_u, f_\theta)
\end{aligned} \tag{12}$$

for all $t \in [0, T]$. In order to estimate the diffusive and stabilization terms, we go back to (9), integrate in time and apply (10):

$$\int_0^t |[\theta_h(\tau)]|_{LPS}^2 \, \mathrm{d}\tau \leq \int_0^t \|f_\theta(\tau)\|_0\|\theta_h(\tau)\|_0 \, \mathrm{d}\tau + \frac{1}{2}\|\theta_{h,0}\|_0^2$$

$$\leq \|\theta_h\|_{L^\infty(0,t;L^2(\Omega))}\|f_\theta\|_{L^1(0,t;L^2(\Omega))} + \frac{1}{2}\|\theta_{h,0}\|_0^2 \leq C_\theta(T,\theta_{h,0},f_\theta)^2.$$

The analogous procedure for $\boldsymbol{u}_h$, starting from (11) and using (12), yields:

$$\begin{aligned}\int_0^t |||\boldsymbol{u}_h(\tau)|||_{LPS}^2 \,\mathrm{d}\tau &\leq \int_0^t \|\boldsymbol{f}_u(\tau) - \beta\boldsymbol{g}\theta_h(\tau)\|_0\|\boldsymbol{u}_h(\tau)\|_0 \,\mathrm{d}\tau + \frac{1}{2}\|\boldsymbol{u}_{h,0}\|_0^2\\ &\leq \|\boldsymbol{u}_h\|_{L^\infty(0,t;L^2(\Omega))}\Big(\|\boldsymbol{f}_u\|_{L^1(0,t;L^2(\Omega))}\\ &\quad + \beta\|\boldsymbol{g}\|_{L^1(0,t;L^\infty(\Omega))}\|\theta_h\|_{L^\infty(0,t;L^2(\Omega))}\Big) + \frac{1}{2}\|\boldsymbol{u}_{h,0}\|_0^2\\ &\leq C_u(T,\boldsymbol{u}_{h,0},\theta_{h,0},\boldsymbol{f}_u,f_\theta)^2.\end{aligned}$$

Remark 1 The discrete inf-sup stability yields a stability estimate of the pressure as well. The above theorem gives us existence of the semi-discrete quantities due to the generalized Peano Theorem. If we assume Lipschitz continuity in time for $\boldsymbol{f}_u$, f_θ and $\boldsymbol{g}$, the Picard-Lindelöf Theorem yields uniqueness of the solution.

4 Quasi-Optimal Semi-Discrete Error Estimates

In this section, we derive quasi-optimal error estimates in the finite element setting introduced above.

For the analysis, we introduce a decomposition of the error into a discretization and a consistency error. Let $(j_u, j_p, j_\theta)\colon \boldsymbol{V}\times Q\times\Theta \to \boldsymbol{V}_h\times Q_h\times\Theta_h$ denote interpolation operators. We introduce

$$\begin{aligned}\boldsymbol{\xi}_{u,h} &:= \boldsymbol{u}-\boldsymbol{u}_h, & \xi_{p,h} &:= p-p_h, & \xi_{\theta,h} &:= \theta-\theta_h,\\ \boldsymbol{\eta}_{u,h} &:= \boldsymbol{u}-j_u\boldsymbol{u}, & \eta_{p,h} &:= p-j_p p, & \eta_{\theta,h} &:= \theta-j_\theta\theta,\\ \boldsymbol{e}_{u,h} &:= j_u\boldsymbol{u}-\boldsymbol{u}_h, & e_{p,h} &:= j_p p-p_h, & e_{\theta,h} &:= j_\theta\theta-\theta_h.\end{aligned} \tag{13}$$

Indeed, the semi-discrete errors are decomposed as $\boldsymbol{\xi}_{u,h} = \boldsymbol{\eta}_{u,h} + \boldsymbol{e}_{u,h}$, $\xi_{p,h} = \eta_{p,h} + e_{p,h}$ and $\xi_{\theta,h} = \eta_{\theta,h} + e_{\theta,h}$.

4.1 Assumptions

For the semi-discrete error analysis, we need the following assumptions for the finite element spaces and stabilization parameters.

Assumption 1 (Interpolation operators) *Assume that for integers $k_u \geq 1$, $k_p \geq 1$, $k_\theta \geq 1$, there are bounded linear interpolation operators $j_u\colon \boldsymbol{V}\to\boldsymbol{V}_h$ preserving the divergence and $j_p\colon Q\to Q_h$ such that for all $M\in\mathcal{M}_h$, for all $\boldsymbol{w}\in\boldsymbol{V}\cap[W^{l_u,2}(\Omega)]^d$ with $1\leq l_u\leq k_u+1$:*

$$\|\boldsymbol{w}-j_u\boldsymbol{w}\|_{0,M} + h_M\|\nabla(\boldsymbol{w}-j_u\boldsymbol{w})\|_{0,M} \leq Ch_M^{l_u}\|\boldsymbol{w}\|_{W^{l_u,2}(\omega_M)} \tag{14}$$

and for all $q\in Q\cap W^{l_p,2}(\Omega)$ with $1\leq l_p\leq k_p+1$:

$$\|q-j_p q\|_{0,M} + h_M\|\nabla(q-j_p q)\|_{0,M} \leq Ch_M^{l_p}\|q\|_{W^{l_p,2}(\omega_M)} \tag{15}$$

on a suitable patch $\omega_M \supseteq M$. *Let for all* $M \in \mathcal{M}_h$

$$\|\boldsymbol{v} - j_u \boldsymbol{v}\|_{\infty,M} \leq C h_M |\boldsymbol{v}|_{W^{1,\infty}(\omega_M)} \qquad \forall \boldsymbol{v} \in [W^{1,\infty}(\Omega)]^d. \tag{16}$$

There is also a bounded linear interpolation operator $j_\theta \colon \Theta \to \Theta_h$ *such that for all* $L \in \mathcal{L}_h$ *and for all* $\psi \in \Theta \cap W^{l_\theta,2}(\Omega)$ *with* $1 \leq l_\theta \leq k_\theta + 1$*:*

$$\|\psi - j_\theta \psi\|_{0,L} + h_L \|\nabla(\psi - j_\theta \psi)\|_{0,L} \leq C h_L^{l_\theta} \|\psi\|_{W^{l_\theta,2}(\omega_L)} \tag{17}$$

on a suitable patch $\omega_L \supseteq L$. *In addition, assume for all* $L \in \mathcal{L}_h$, $M \in \mathcal{M}_h$

$$\begin{aligned} \|\psi - j_\theta \psi\|_{\infty,L} &\leq C h_L |\psi|_{W^{1,\infty}(\omega_L)} && \forall \psi \in W^{1,\infty}(\Omega), \\ \|\psi - j_\theta \psi\|_{\infty,M} &\leq C h_M |\psi|_{W^{1,\infty}(\omega_M)} && \forall \psi \in W^{1,\infty}(\Omega). \end{aligned} \tag{18}$$

The last property (18) for j_θ holds due to the fact that all $M \in \mathcal{M}_h$ and $L \in \mathcal{L}_h$ are formed as a conjunction of at most $n_{\mathcal{T}_h} < \infty$ cells $T \in \mathcal{T}_h$. If the interpolator is constructed such that the above estimates hold true on all $T \in \mathcal{T}_h$, the same localized estimates hold on $M \in \mathcal{M}_h$ and $L \in \mathcal{L}_h$.

Assumption 2 (Local inverse inequality) *Let the FE spaces* $[Y_h^u]^d$ *for the velocity and* Y_h^θ *for the temperature satisfy the local inverse inequalities*

$$\begin{aligned} \|\nabla \boldsymbol{w}_h\|_{0,M} &\leq C h_M^{-1} \|\boldsymbol{w}_h\|_{0,M} \quad \forall \boldsymbol{w}_h \in [Y_h^u]^d,\ M \in \mathcal{M}_h, \\ \|\nabla \psi_h\|_{0,L} &\leq C h_L^{-1} \|\psi_h\|_{0,L} \quad \forall \psi_h \in Y_h^\theta,\ L \in \mathcal{L}_h. \end{aligned}$$

Assumption 3 (Properties of the fluctuation operators) *Assume that for given integers* k_u, $k_\theta \geq 1$, *there are* $s_u \in \{0, \cdots, k_u\}$ *and* $s_\theta \in \{0, \cdots, k_\theta\}$ *such that the fluctuation operators* $\kappa_M^u = Id - \pi_M^u$ *and* $\kappa_L^\theta = Id - \pi_L^\theta$ *provide the following approximation properties: There is* $C > 0$ *such that for* $\boldsymbol{w} \in [W^{l,2}(M)]^d$ *with* $M \in \mathcal{M}_h$, $l = 0, \ldots, s_u$ *and for* $\psi \in W^{r,2}(L)$ *with* $L \in \mathcal{L}_h$, $r = 0, \ldots, s_\theta$, *it holds*

$$\|\kappa_M^u \boldsymbol{w}\|_{0,M} \leq C h_M^l \|\boldsymbol{w}\|_{W^{l,2}(M)}, \qquad \|\kappa_L^\theta \psi\|_{0,L} \leq C h_L^r \|\psi\|_{W^{r,2}(L)}.$$

Note that this is a property of the coarse spaces $\boldsymbol{D}_M^u$ and D_L^θ and is always true for $s_u = s_\theta = 0$.

Furthermore, we need to satisfy some requirements on the stabilization parameters:

Assumption 4 (Parameter bounds) *Assume that for all* $M \in \mathcal{M}_h$, $E \in \mathcal{E}_h$ *and* $L \in \mathcal{L}_h$*:*

$$\begin{aligned} \max_{M \in \mathcal{M}_h} \tau_M^u(\boldsymbol{u}_M) |\boldsymbol{u}_M|^2 &\in L^\infty(0,T), && \tau_M^u(\boldsymbol{u}_M) \geq 0, \\ \max_{M \in \mathcal{M}_h} (\gamma_M(\boldsymbol{u}_M) + \gamma_M(\boldsymbol{u}_M)^{-1}) &\in L^\infty(0,T), && \gamma_M(\boldsymbol{u}_M) \geq 0, \\ \max_{L \in \mathcal{L}_h} \tau_L^\theta(\boldsymbol{u}_L) |\boldsymbol{u}_L|^2 &\in L^\infty(0,T), && \tau_L^\theta(\boldsymbol{u}_L) \geq 0. \end{aligned}$$

4.2 Velocity and Temperature Estimates

This gives rise to the following quasi-optimal semi-discrete error estimate for the LPS-model.

Theorem 2 *Let* $(\boldsymbol{u}, p, \theta)\colon [0,T] \to \boldsymbol{V}^{div} \times Q \times \Theta$, $(\boldsymbol{u}_h, p_h, \theta_h)\colon [0,T] \to \boldsymbol{V}_h^{div} \times Q_h \times \Theta_h$ *be solutions of (2)-(3) and (7)-(8) satisfying*

$$\begin{aligned}
&\boldsymbol{u} \in L^\infty(0,T;[W^{1,\infty}(\Omega)]^d), \quad \partial_t \boldsymbol{u} \in L^2(0,T;[L^2(\Omega)]^d), \qquad p \in L^2(0,T;Q \cap C(\Omega)),\\
&\theta \in L^\infty(0,T;W^{1,\infty}(\Omega)), \qquad \partial_t \theta \in L^2(0,T;L^2(\Omega)), \qquad \boldsymbol{u}_h \in L^\infty(0,T;[L^\infty(\Omega)]^d).
\end{aligned}$$

Let Assumptions 1, 2 and 4 be valid and $\boldsymbol{u}_h(0) = j_u \boldsymbol{u}_0$, $\theta_h(0) = j_\theta \theta_0$. *We obtain for* $\boldsymbol{e}_{u,h} = j_u \boldsymbol{u} - \boldsymbol{u}_h$, $e_{\theta,h} = j_\theta \theta - \theta_h$ *of the LPS-method (7)-(8) for all* $0 \le t \le T$*:*

$$\begin{aligned}
&\|\boldsymbol{e}_{u,h}\|^2_{L^\infty(0,t;L^2(\Omega))} + \|e_{\theta,h}\|^2_{L^\infty(0,t;L^2(\Omega))}\\
&\quad + \int_0^t \left(|||\boldsymbol{e}_{u,h}(\tau)|||^2_{LPS} + |[e_{\theta,h}(\tau)]|^2_{LPS} \right) \mathrm{d}\tau\\
&\lesssim \int_0^t e^{C_{G,h}(\boldsymbol{u},\theta,\boldsymbol{u}_h)(t-\tau)} \Bigg\{ \sum_{M \in \mathcal{M}_h} \Big[(\nu + \tau_M^u |\boldsymbol{u}_M|^2 + \gamma_M d) \|\nabla \boldsymbol{\eta}_{u,h}(\tau)\|^2_{0,M}\\
&\quad + h_M^{-2} \|\boldsymbol{\eta}_{u,h}(\tau)\|^2_{0,M} + \|\partial_t \boldsymbol{\eta}_{u,h}(\tau)\|^2_{0,M}\\
&\quad + \tau_M^u |\boldsymbol{u}_M|^2 \|\kappa_M^u(\nabla \boldsymbol{u})(\tau)\|^2_{0,M} + \min\left(\frac{d}{\nu}, \frac{1}{\gamma_M}\right) \|\eta_{p,h}(\tau)\|^2_{0,M} \Big]\\
&\quad + \sum_{L \in \mathcal{L}_h} \Big[\|\partial_t \eta_{\theta,h}(\tau)\|_0^2 + \left(h_L^{-2} + \beta \|\boldsymbol{g}\|_{\infty,L}\right) \|\eta_{\theta,h}(\tau)\|^2_{0,L}\\
&\quad + \left(\alpha + \tau_L^\theta |\boldsymbol{u}_L|^2\right) \|\nabla \eta_{\theta,h}(\tau)\|^2_{0,L} + \tau_L^\theta |\boldsymbol{u}_L|^2 \|\kappa_L^\theta(\nabla\theta)(\tau)\|^2_{0,L} \Big] \Bigg\} \mathrm{d}\tau
\end{aligned}$$

with $(\boldsymbol{\eta}_{u,h}, \eta_{p,h}, \eta_{\theta,h}) = (\boldsymbol{u} - j_u \boldsymbol{u}, p - j_p p, \theta - j_\theta \theta)$ *and the Gronwall constant*

$$\begin{aligned}
C_{G,h}(\boldsymbol{u},\theta,\boldsymbol{u}_h) = 1 &+ \beta\|\boldsymbol{g}\|_\infty + |\boldsymbol{u}|_{W^{1,\infty}(\Omega)} + |\theta|_{W^{1,\infty}(\Omega)} + \|\boldsymbol{u}_h\|^2_\infty\\
&+ \max_{M \in \mathcal{M}_h} \{h_M^2 |\boldsymbol{u}|^2_{W^{1,\infty}(M)}\} + \max_{M \in \mathcal{M}_h} \left\{ \frac{h_M^2}{\gamma_M} |\boldsymbol{u}|^2_{W^{1,\infty}(M)} \right\}\\
&+ \max_{M \in \mathcal{M}_h} \{\gamma_M^{-1} \|\boldsymbol{u}\|^2_{\infty,M}\} + \max_{M \in \mathcal{M}_h} \{h_M^2 |\theta|^2_{W^{1,\infty}(M)}\}\\
&+ \max_{M \in \mathcal{M}_h} \left\{ \frac{h_M^2}{\gamma_M} |\theta|^2_{W^{1,\infty}(M)} \right\} + \max_{M \in \mathcal{M}_h} \{\gamma_M^{-1} \|\theta\|^2_{\infty,M}\}.
\end{aligned} \tag{19}$$

Proof We use the interpolation operators $j_u\colon \boldsymbol{V} \to \boldsymbol{V}_h$ preserving the divergence, $j_\theta\colon \Theta \to \Theta_h$ and $j_p\colon Q \to Q_h$ from Assumption 1. Note that $j_u \boldsymbol{u} \in \boldsymbol{V}_h^{div}$. Subtracting (7) from (2), testing with $(\boldsymbol{v}_h, q_h) = (\boldsymbol{e}_{u,h}, 0) \in \boldsymbol{V}_h^{div} \times Q_h$ and using (13) lead to an error equation for the velocity:

$$\begin{aligned}
0 &= (\partial_t(\boldsymbol{u} - \boldsymbol{u}_h), \boldsymbol{e}_{u,h}) + (\nu\nabla(\boldsymbol{u} - \boldsymbol{u}_h), \nabla \boldsymbol{e}_{u,h}) - (p - p_h, \nabla \cdot \boldsymbol{e}_{u,h}) + c_u(\boldsymbol{u}; \boldsymbol{u}, \boldsymbol{e}_{u,h})\\
&\quad - c_u(\boldsymbol{u}_h; \boldsymbol{u}_h, \boldsymbol{e}_{u,h}) - s_u(\boldsymbol{u}_h; \boldsymbol{u}_h, \boldsymbol{e}_{u,h}) - t_h(\boldsymbol{u}_h; \boldsymbol{u}_h, \boldsymbol{e}_{u,h}) + (\beta \boldsymbol{g}(\theta - \theta_h), \boldsymbol{e}_{u,h})\\
&= (\partial_t \boldsymbol{\eta}_{u,h}, \boldsymbol{e}_{u,h}) + (\partial_t \boldsymbol{e}_{u,h}, \boldsymbol{e}_{u,h}) + (\nu \nabla \boldsymbol{\eta}_{u,h}, \nabla \boldsymbol{e}_{u,h}) + (\nu \nabla \boldsymbol{e}_{u,h}, \nabla \boldsymbol{e}_{u,h})\\
&\quad - (\eta_{p,h}, \nabla \cdot \boldsymbol{e}_{u,h}) + c_u(\boldsymbol{u}; \boldsymbol{u}, \boldsymbol{e}_{u,h}) - c_u(\boldsymbol{u}_h; \boldsymbol{u}_h, \boldsymbol{e}_{u,h}) + s_u(\boldsymbol{u}_h; \boldsymbol{e}_{u,h}, \boldsymbol{e}_{u,h})
\end{aligned}$$

$$
\begin{aligned}
&+ s_u(\boldsymbol{u}_h;\boldsymbol{\eta}_{u,h},\boldsymbol{e}_{u,h}) - s_u(\boldsymbol{u}_h;\boldsymbol{u},\boldsymbol{e}_{u,h}) + t_h(\boldsymbol{u}_h;\boldsymbol{e}_{u,h},\boldsymbol{e}_{u,h}) - t_h(\boldsymbol{u}_h;j_u\boldsymbol{u},\boldsymbol{e}_{u,h})\\
&+ \beta(\boldsymbol{g}e_{\theta,h},\boldsymbol{e}_{u,h}) + \beta(\boldsymbol{g}\eta_{\theta,h},\boldsymbol{e}_{u,h}),
\end{aligned}
$$

where we used $(e_{p,h},\nabla\cdot\boldsymbol{e}_{u,h}) = 0$ due to $\boldsymbol{e}_{u,h}\in\boldsymbol{V}_h^{div}$. With the definition of $|||\cdot|||_{LPS}$ and the fact that $(\nabla\cdot\boldsymbol{u},q)=0$ for all $q\in L^2(\Omega)$, this implies

$$
\begin{aligned}
&\frac{1}{2}\partial_t\|\boldsymbol{e}_{u,h}\|_0^2 + |||\boldsymbol{e}_{u,h}|||_{LPS}^2\\
&= -(\partial_t\boldsymbol{\eta}_{u,h},\boldsymbol{e}_{u,h}) - \nu(\nabla\boldsymbol{\eta}_{u,h},\nabla\boldsymbol{e}_{u,h}) + (\eta_{p,h},\nabla\cdot\boldsymbol{e}_{u,h}) + c_u(\boldsymbol{u}_h;\boldsymbol{u}_h,\boldsymbol{e}_{u,h})\\
&\quad - c_u(\boldsymbol{u};\boldsymbol{u},\boldsymbol{e}_{u,h}) - s_u(\boldsymbol{u}_h;\boldsymbol{\eta}_{u,h},\boldsymbol{e}_{u,h}) - t_h(\boldsymbol{u}_h;\boldsymbol{\eta}_{u,h},\boldsymbol{e}_{u,h})\\
&\quad + s_u(\boldsymbol{u}_h;\boldsymbol{u},\boldsymbol{e}_{u,h}) - \beta(\boldsymbol{g}e_{\theta,h},\boldsymbol{e}_{u,h}) - \beta(\boldsymbol{g}\eta_{\theta,h},\boldsymbol{e}_{u,h}).
\end{aligned}
$$

The right-hand side terms are bounded as:

$$
\begin{aligned}
-(\partial_t\boldsymbol{\eta}_{u,h},\boldsymbol{e}_{u,h}) &\le \|\partial_t\boldsymbol{\eta}_{u,h}\|_0\|\boldsymbol{e}_{u,h}\|_0 \le \frac{1}{4}\|\partial_t\boldsymbol{\eta}_{u,h}\|_0^2 + \|\boldsymbol{e}_{u,h}\|_0^2,\\
-\nu(\nabla\boldsymbol{\eta}_{u,h},\nabla\boldsymbol{e}_{u,h}) &\le \sqrt{\nu}\|\nabla\boldsymbol{\eta}_{u,h}\|_0|||\boldsymbol{e}_{u,h}|||_{LPS},\\
(\eta_{p,h},\nabla\cdot\boldsymbol{e}_{u,h}) &\le \Big(\sum_{M\in\mathcal{M}_h}\min\Big(\frac{d}{\nu},\frac{1}{\gamma_M}\Big)\|\eta_{p,h}\|_{0,M}^2\Big)^{1/2}|||\boldsymbol{e}_{u,h}|||_{LPS},\\
-s_u(\boldsymbol{u}_h;\boldsymbol{\eta}_{u,h},\boldsymbol{e}_{u,h}) &\le \Big(\sum_{M\in\mathcal{M}_h}\tau_M^u|\boldsymbol{u}_M|^2\|\nabla\boldsymbol{\eta}_{u,h}\|_{0,M}^2\Big)^{1/2}|||\boldsymbol{e}_{u,h}|||_{LPS},\\
-t_h(\boldsymbol{u}_h;\boldsymbol{\eta}_{u,h},\boldsymbol{e}_{u,h}) &\le \Big(\sum_{M\in\mathcal{M}_h}\gamma_M d\|\nabla\boldsymbol{\eta}_{u,h}\|_{0,M}^2\Big)^{1/2}|||\boldsymbol{e}_{u,h}|||_{LPS},\\
s_u(\boldsymbol{u}_h;\boldsymbol{u},\boldsymbol{e}_{u,h}) &\le \Big(\sum_{M\in\mathcal{M}_h}\tau_M^u|\boldsymbol{u}_M|^2\|\kappa_M^u(\nabla\boldsymbol{u})\|_{0,M}^2\Big)^{1/2}|||\boldsymbol{e}_{u,h}|||_{LPS},\\
|\beta(\boldsymbol{g}e_{\theta,h},\boldsymbol{e}_{u,h})| &\le \frac{1}{4}\beta\|\boldsymbol{g}\|_\infty\|\boldsymbol{e}_{u,h}\|_0^2 + \beta\|\boldsymbol{g}\|_\infty\|e_{\theta,h}\|_0^2\\
|\beta(\boldsymbol{g}\eta_{\theta,h},\boldsymbol{e}_{u,h})| &\le \frac{3}{4}\beta\|\boldsymbol{g}\|_\infty\|\boldsymbol{e}_{u,h}\|_0^2 + \frac{1}{3}\beta\|\boldsymbol{g}\|_\infty\|\eta_{\theta,h}\|_0^2.
\end{aligned}
$$

Therefore,

$$
\begin{aligned}
&\frac{1}{2}\partial_t\|\boldsymbol{e}_{u,h}\|_0^2 + |||\boldsymbol{e}_{u,h}|||_{LPS}^2\\
&\le \frac{1}{4}\|\partial_t\boldsymbol{\eta}_{u,h}\|_0^2 + \|\boldsymbol{e}_{u,h}\|_0^2 + c_u(\boldsymbol{u}_h;\boldsymbol{u}_h,\boldsymbol{e}_{u,h}) - c_u(\boldsymbol{u};\boldsymbol{u},\boldsymbol{e}_{u,h})\\
&\quad + \Bigg[\sqrt{\nu}\|\nabla\boldsymbol{\eta}_{u,h}\|_0 + \Big(\sum_{M\in\mathcal{M}_h}\tau_M^u|\boldsymbol{u}_M|^2\|\nabla\boldsymbol{\eta}_{u,h}\|_{0,M}^2\Big)^{1/2}\\
&\qquad + \Big(\sum_{M\in\mathcal{M}_h}\gamma_M d\|\nabla\boldsymbol{\eta}_{u,h}\|_{0,M}^2\Big)^{1/2} + \Big(\sum_{M\in\mathcal{M}_h}\min\Big(\frac{d}{\nu},\frac{1}{\gamma_M}\Big)\|\eta_{p,h}\|_{0,M}^2\Big)^{1/2}\\
&\qquad + \Big(\sum_{M\in\mathcal{M}_h}\tau_M^u|\boldsymbol{u}_M|^2\|\kappa_M^u(\nabla\boldsymbol{u})\|_{0,M}^2\Big)^{1/2}\Bigg]|||\boldsymbol{e}_{u,h}|||_{LPS}\\
&\quad + \beta\|\boldsymbol{g}\|_\infty\Big(\|e_{\theta,h}\|_0^2 + \|\boldsymbol{e}_{u,h}\|_0^2\Big) + \frac{\beta\|\boldsymbol{g}\|_\infty}{3}\|\eta_{\theta,h}\|_0^2
\end{aligned}
$$

and thus via Young's inequality

$$
\begin{aligned}
&\frac{1}{2}\partial_t\|\boldsymbol{e}_{u,h}\|_0^2 + (1-2\epsilon)|||\boldsymbol{e}_{u,h}|||_{LPS}^2 \\
&\leq \frac{1}{4}\|\partial_t\boldsymbol{\eta}_{u,h}\|_0^2 + \|\boldsymbol{e}_{u,h}\|_0^2 + \left[c_u(\boldsymbol{u}_h;\boldsymbol{u}_h,\boldsymbol{e}_{u,h}) - c_u(\boldsymbol{u};\boldsymbol{u},\boldsymbol{e}_{u,h})\right] \\
&\quad + \frac{5}{8\epsilon}\sum_{M\in\mathcal{M}_h}\Big[\big(\nu + \tau_M^u|\boldsymbol{u}_M|^2 + \gamma_M d\big)\|\nabla\boldsymbol{\eta}_{u,h}\|_{0,M}^2 \\
&\qquad\qquad + \min\Big(\frac{d}{\nu},\frac{1}{\gamma_M}\Big)\|\eta_{p,h}\|_{0,M}^2 + \tau_M^u|\boldsymbol{u}_M|^2\|\kappa_M^u(\nabla\boldsymbol{u})\|_{0,M}^2\Big] \\
&\quad + \beta\|\boldsymbol{g}\|_\infty\Big(\|e_{\theta,h}\|_0^2 + \|\boldsymbol{e}_{u,h}\|_0^2\Big) + \frac{\beta\|\boldsymbol{g}\|_\infty}{3}\|\eta_{\theta,h}\|_0^2.
\end{aligned}
\tag{20}
$$

Lemma 1 yields for the convective terms:

$$
\begin{aligned}
&c_u(\boldsymbol{u};\boldsymbol{u},\boldsymbol{e}_{u,h}) - c_u(\boldsymbol{u}_h;\boldsymbol{u}_h,\boldsymbol{e}_{u,h}) \\
&\leq \frac{C}{\epsilon}\sum_{M\in\mathcal{M}_h}\frac{1}{h_M^2}\|\boldsymbol{\eta}_{u,h}\|_{0,M}^2 + 3\epsilon|||\boldsymbol{\eta}_{u,h}|||_{LPS}^2 + 3\epsilon|||\boldsymbol{e}_{u,h}|||_{LPS}^2 \\
&\quad + \Bigg[|\boldsymbol{u}|_{W^{1,\infty}(\Omega)} + \epsilon\max_{M\in\mathcal{M}_h}\{h_M^2|\boldsymbol{u}|_{W^{1,\infty}(M)}^2\} + \frac{C}{\epsilon}\max_{M\in\mathcal{M}_h}\Big\{\frac{h_M^2}{\gamma_M}|\boldsymbol{u}|_{W^{1,\infty}(M)}^2\Big\} \\
&\qquad + \frac{C}{\epsilon}\max_{M\in\mathcal{M}_h}\{\gamma_M^{-1}\|\boldsymbol{u}\|_{\infty,M}^2\} + \epsilon\|\boldsymbol{u}_h\|_\infty^2\Bigg]\|\boldsymbol{e}_{u,h}\|_0^2
\end{aligned}
$$

We incorporate this into (20) and obtain with a constant C independent of the problem parameters, h_M, h_L, the solutions and ϵ

$$
\begin{aligned}
&\frac{1}{2}\partial_t\|\boldsymbol{e}_{u,h}\|_0^2 + (1-5\epsilon)|||\boldsymbol{e}_{u,h}|||_{LPS}^2 \\
&\leq \frac{1}{4}\|\partial_t\boldsymbol{\eta}_{u,h}\|_0^2 + \frac{C}{\epsilon}\sum_{M\in\mathcal{M}_h}\frac{1}{h_M^2}\|\boldsymbol{\eta}_{u,h}\|_{0,M}^2 \\
&\quad + \Bigg[1 + \beta\|\boldsymbol{g}\|_\infty + |\boldsymbol{u}|_{W^{1,\infty}(\Omega)} + \epsilon\max_{M\in\mathcal{M}_h}\{h_M^2|\boldsymbol{u}|_{W^{1,\infty}(M)}^2\} \\
&\qquad + \frac{C}{\epsilon}\max_{M\in\mathcal{M}_h}\Big\{\frac{h_M^2}{\gamma_M}|\boldsymbol{u}|_{W^{1,\infty}(M)}^2\Big\} \\
&\qquad + \frac{C}{\epsilon}\max_{M\in\mathcal{M}_h}\{\gamma_M^{-1}\|\boldsymbol{u}\|_{\infty,M}^2\} + \epsilon\|\boldsymbol{u}_h\|_\infty^2\Bigg]\|\boldsymbol{e}_{u,h}\|_0^2 \\
&\quad + \frac{C}{\epsilon}\sum_{M\in\mathcal{M}_h}\Bigg[\big(\nu + \tau_M^u|\boldsymbol{u}_M|^2 + \gamma_M d\big)\|\nabla\boldsymbol{\eta}_{u,h}\|_{0,M}^2 \\
&\qquad\qquad + \min\Big(\frac{d}{\nu},\frac{1}{\gamma_M}\Big)\|\eta_{p,h}\|_{0,M}^2 + \tau_M^u|\boldsymbol{u}_M|^2\|\kappa_M^u(\nabla\boldsymbol{u})\|_{0,M}^2\Bigg] \\
&\quad + \beta\|\boldsymbol{g}\|_\infty\|e_{\theta,h}\|_0^2 + C\beta\|\boldsymbol{g}\|_\infty\|\eta_{\theta,h}\|_0^2.
\end{aligned}
\tag{21}
$$

Now, subtracting (8) from (3) with $\psi_h = e_{\theta,h} \in \Theta_h$ as a test function leads to

$$
\frac{1}{2}\partial_t\|e_{\theta,h}\|_0^2 + |[e_{\theta,h}]|_{LPS}^2
$$

$$
\begin{aligned}
&= -(\partial_t \eta_{\theta,h}, e_{\theta,h}) - \alpha(\nabla \eta_{\theta,h}, \nabla e_{\theta,h}) + c_\theta(\boldsymbol{u}_h; \theta_h, e_{\theta,h}) \\
&\quad - c_\theta(\boldsymbol{u}; \theta, e_{\theta,h}) - s_\theta(\boldsymbol{u}_h; \eta_{\theta,h}, e_{\theta,h}) + s_\theta(\boldsymbol{u}_h; \theta, e_{\theta,h}).
\end{aligned}
$$

With estimates for the interpolation terms and Young's inequality, we have

$$
\begin{aligned}
&\frac{1}{2}\partial_t \|e_{\theta,h}\|_0^2 + (1-2\epsilon)|[e_{\theta,h}]|_{LPS}^2 \\
&\leq \frac{1}{4}\|\partial_t \eta_{\theta,h}\|_0^2 + \|e_{\theta,h}\|_0^2 + c_\theta(\boldsymbol{u}_h; \theta_h, e_{\theta,h}) - c_\theta(\boldsymbol{u}; \theta, e_{\theta,h}) \\
&\quad + \frac{3}{8\epsilon} \sum_{L \in \mathcal{L}_h} \Big[\big(\alpha + \tau_L^\theta |\boldsymbol{u}_L|^2\big) \|\nabla \eta_{\theta,h}\|_{0,L}^2 + \tau_L^\theta |\boldsymbol{u}_L|^2 \|\kappa_L^\theta(\nabla\theta)\|_{0,L}^2 \Big].
\end{aligned} \tag{22}
$$

The combination of (22) and the difference of the convective terms in the Fourier equation according to Lemma 1 with a constant C independent of the problem parameters, h_M, h_L, the solutions and ϵ gives

$$
\begin{aligned}
&\frac{1}{2}\partial_t \|e_{\theta,h}\|_0^2 + (1-8\epsilon)|[e_{\theta,h}]|_{LPS}^2 \\
&\leq \frac{1}{4}\|\partial_t \eta_{\theta,h}\|_0^2 + \frac{C}{\epsilon} \sum_{L \in \mathcal{L}_h} \frac{1}{h_L^2} \|\eta_{\theta,h}\|_{0,L}^2 + \frac{C}{\epsilon} \sum_{M \in \mathcal{M}_h} \frac{1}{h_M^2} \|\boldsymbol{\eta}_{u,h}\|_{0,M}^2 \\
&\quad + 3\epsilon |||\boldsymbol{\eta}_{u,h}|||_{LPS}^2 + 3\epsilon |||\boldsymbol{e}_{u,h}|||_{LPS}^2 + \frac{1}{2}|\theta|_{W^{1,\infty}(\Omega)} \|\boldsymbol{e}_{u,h}\|_0^2 \\
&\quad + \Bigg[1 + \frac{1}{2}|\theta|_{W^{1,\infty}(\Omega)} + \epsilon \|\boldsymbol{u}_h\|_\infty^2 + \epsilon \max_{M \in \mathcal{M}_h} \{h_M^2 |\theta|_{W^{1,\infty}(M)}^2\} \\
&\qquad + \frac{C}{\epsilon} \max_{M \in \mathcal{M}_h} \Big\{ \frac{h_M^2}{\gamma_M} |\theta|_{W^{1,\infty}(M)}^2 \Big\} + \frac{C}{\epsilon} \max_{M \in \mathcal{M}_h} \{\gamma_M^{-1} \|\theta\|_{\infty,M}^2\} \Bigg] \|e_{\theta,h}\|_0^2 \\
&\quad + \frac{C}{\epsilon} \sum_{L \in \mathcal{L}_h} \Big[\big(\alpha + \tau_L^\theta |\boldsymbol{u}_L|^2\big) \|\nabla \eta_{\theta,h}\|_{0,L}^2 + \tau_L^\theta |\boldsymbol{u}_L|^2 \|\kappa_L^\theta(\nabla\theta)\|_{0,L}^2 \Big].
\end{aligned} \tag{23}
$$

Note that

$$
|||\boldsymbol{\eta}_{u,h}|||_{LPS}^2 \leq \sum_{M \in \mathcal{M}_h} \big(\nu + \tau_M^u |\boldsymbol{u}_M|^2 + \gamma_M d\big) \|\nabla \boldsymbol{\eta}_{u,h}\|_{0,M}^2.
$$

Adding (21) and (23) results in

$$
\begin{aligned}
&\frac{1}{2}\partial_t \|\boldsymbol{e}_{u,h}\|_0^2 + (1-8\epsilon)|||\boldsymbol{e}_{u,h}|||_{LPS}^2 + \frac{1}{2}\partial_t \|e_{\theta,h}\|_0^2 + (1-8\epsilon)|[e_{\theta,h}]|_{LPS}^2 \\
&\leq \frac{1}{4}\|\partial_t \boldsymbol{\eta}_{u,h}\|_0^2 + \frac{1}{4}\|\partial_t \eta_{\theta,h}\|_0^2 + \frac{C}{\epsilon} \sum_{M \in \mathcal{M}_h} \frac{1}{h_M^2} \|\boldsymbol{\eta}_{u,h}\|_{0,M}^2 \\
&\quad + \Big[1 + \beta \|\boldsymbol{g}\|_\infty + |\boldsymbol{u}|_{W^{1,\infty}(\Omega)} + \epsilon \max_{M \in \mathcal{M}_h} \{h_M^2 |\boldsymbol{u}|_{W^{1,\infty}(M)}^2\} \\
&\qquad + \frac{C}{\epsilon} \max_{M \in \mathcal{M}_h} \Big\{ \frac{h_M^2}{\gamma_M} |\boldsymbol{u}|_{W^{1,\infty}(M)}^2 \Big\} + \epsilon \|\boldsymbol{u}_h\|_\infty^2 \\
&\qquad + \frac{C}{\epsilon} \max_{M \in \mathcal{M}_h} \{\gamma_M^{-1} \|\boldsymbol{u}\|_{\infty,M}^2\} + \frac{1}{2}|\theta|_{W^{1,\infty}(\Omega)} \Big] \|\boldsymbol{e}_{u,h}\|_0^2 \\
&\quad + \left(\frac{C}{\epsilon} + C\epsilon \right) \sum_{M \in \mathcal{M}_h} \big(\nu + \tau_M^u |\boldsymbol{u}_M|^2 + \gamma_M d\big) \|\nabla \boldsymbol{\eta}_{u,h}\|_{0,M}^2
\end{aligned}
$$

$$
\begin{aligned}
&+ \frac{C}{\epsilon} \sum_{M\in\mathcal{M}_h} \Big[\min\Big(\frac{d}{\nu}, \frac{1}{\gamma_M}\Big) \|\eta_{p,h}\|_{0,M}^2 + \tau_M^u |\boldsymbol{u}_M|^2 \|\kappa_M^u(\nabla \boldsymbol{u})\|_{0,M}^2 \Big] \\
&+ \sum_{L\in\mathcal{L}_h} \left(\frac{C}{\epsilon} \frac{1}{h_L^2} + C\beta \|\boldsymbol{g}\|_{\infty,L} \right) \|\eta_{\theta,h}\|_{0,L}^2 \\
&+ \Bigg[1 + \frac{1}{2}|\theta|_{W^{1,\infty}(\Omega)} + \epsilon \|\boldsymbol{u}_h\|_\infty^2 + \beta \|\boldsymbol{g}\|_\infty + \epsilon \max_{M\in\mathcal{M}_h} \{h_M^2 |\theta|_{W^{1,\infty}(M)}^2\} \\
&\qquad + \frac{C}{\epsilon} \max_{M\in\mathcal{M}_h} \Big\{ \frac{h_M^2}{\gamma_M} |\theta|_{W^{1,\infty}(M)}^2 \Big\} + \frac{C}{\epsilon} \max_{M\in\mathcal{M}_h} \{\gamma_M^{-1} \|\theta\|_{\infty,M}^2\} \Bigg] \|e_{\theta,h}\|_0^2 \\
&+ \frac{C}{\epsilon} \sum_{L\in\mathcal{L}_h} \Big[\big(\alpha + \tau_L^\theta |\boldsymbol{u}_L|^2\big) \|\nabla \eta_{\theta,h}\|_{0,L}^2 + \tau_L^\theta |\boldsymbol{u}_L|^2 \|\kappa_L^\theta(\nabla\theta)\|_{0,L}^2 \Big].
\end{aligned}
$$

We choose $\epsilon = \frac{1}{18}$ and get (where $\lesssim$ indicates that the left-hand side is smaller or equal than a generic constant times the right-hand side)

$$
\begin{aligned}
&\partial_t \|\boldsymbol{e}_{u,h}\|_0^2 + |||(\boldsymbol{e}_{u,h}, e_{p,h})|||_{LPS}^2 + \partial_t \|e_{\theta,h}\|_0^2 + |[e_{\theta,h}]|_{LPS}^2 \\
&\lesssim \|\partial_t \boldsymbol{\eta}_{u,h}\|_0^2 + \|\partial_t \eta_{\theta,h}\|_0^2 + \sum_{M\in\mathcal{M}_h} \frac{1}{h_M^2} \|\boldsymbol{\eta}_{u,h}\|_{0,M}^2 \\
&\quad + \Big[1 + \beta\|\boldsymbol{g}\|_\infty + |\boldsymbol{u}|_{W^{1,\infty}(\Omega)} + \max_{M\in\mathcal{M}_h} \{h_M^2 |\boldsymbol{u}|_{W^{1,\infty}(M)}^2\} + \|\boldsymbol{u}_h\|_\infty^2 \\
&\qquad + \max_{M\in\mathcal{M}_h} \Big\{ \frac{h_M^2}{\gamma_M} |\boldsymbol{u}|_{W^{1,\infty}(M)}^2 \Big\} + \max_{M\in\mathcal{M}_h} \{\gamma_M^{-1} \|\boldsymbol{u}\|_{\infty,M}^2\} + |\theta|_{W^{1,\infty}(\Omega)} \Big] \|\boldsymbol{e}_{u,h}\|_0^2 \\
&\quad + \sum_{M\in\mathcal{M}_h} \big(\nu + \tau_M^u |\boldsymbol{u}_M|^2 + \gamma_M d\big) \|\nabla \boldsymbol{\eta}_{u,h}\|_{0,M}^2 \\
&\quad + \sum_{M\in\mathcal{M}_h} \Big[\min\Big(\frac{d}{\nu}, \frac{1}{\gamma_M}\Big) \|\eta_{p,h}\|_{0,M}^2 + \tau_M^u |\boldsymbol{u}_M|^2 \|\kappa_M^u(\nabla \boldsymbol{u})\|_{0,M}^2 \Big] \\
&\quad + \sum_{L\in\mathcal{L}_h} \left(\frac{1}{h_L^2} + \beta \|\boldsymbol{g}\|_{\infty,L} \right) \|\eta_{\theta,h}\|_{0,L}^2 \\
&\quad + \Bigg[1 + |\theta|_{W^{1,\infty}(\Omega)} + \|\boldsymbol{u}_h\|_\infty^2 + \beta \|\boldsymbol{g}\|_\infty + \max_{M\in\mathcal{M}_h} \{h_M^2 |\theta|_{W^{1,\infty}(M)}^2\} \\
&\qquad + \max_{M\in\mathcal{M}_h} \Big\{ \frac{h_M^2}{\gamma_M} |\theta|_{W^{1,\infty}(M)}^2 \Big\} + \max_{M\in\mathcal{M}_h} \{\gamma_M^{-1} \|\theta\|_{\infty,M}^2\} \Bigg] \|e_{\theta,h}\|_0^2 \\
&\quad + \sum_{L\in\mathcal{L}_h} \Big[\big(\alpha + \tau_L^\theta |\boldsymbol{u}_L|^2\big) \|\nabla \eta_{\theta,h}\|_{0,L}^2 + \tau_L^\theta |\boldsymbol{u}_L|^2 \|\kappa_L^\theta(\nabla\theta)\|_{0,L}^2 \Big].
\end{aligned}
$$

We require that all the terms on the right-hand side are integrable in time. This holds due to the regularity assumptions on $\boldsymbol{u}$ and θ, Assumption 4, $\boldsymbol{g} \in L^\infty(0,T;[L^\infty(\Omega)]^d)$ and the fact that the fluctuation operators are bounded. Application of Gronwall's Lemma for $\|(\boldsymbol{e}_{u,h}, e_{\theta,h})\|_0^2 := \|\boldsymbol{e}_{u,h}\|_0^2 + \|e_{\theta,h}\|_0^2$ defined in Theorem 2 gives the claim since the initial error $(\boldsymbol{e}_{u,h}, e_{\theta,h})(0)$ vanishes.

Corollary 1 *Consider a solution* $(\boldsymbol{u}, p, \theta)\colon [0,T] \to \boldsymbol{V}^{div} \times Q \times \Theta$ *of (2)-(3) satisfying*

$$
\boldsymbol{u} \in L^\infty(0,T;[W^{1,\infty}(\Omega)]^d) \cap L^2(0,T;[W^{k_u+1,2}(\Omega)]^d),
$$

$$\begin{aligned}\partial_t \boldsymbol{u} &\in L^2(0,T;[W^{k_u,2}(\Omega)]^d),\\ p &\in L^2(0,T;W^{k_p+1,2}(\Omega)\cap C(\Omega)),\\ \theta &\in L^\infty(0,T;W^{1,\infty}(\Omega))\cap L^2(0,T;W^{k_\theta+1,2}(\Omega)),\\ \partial_t\theta &\in L^2(0,T;W^{k_\theta,2}(\Omega))\end{aligned}$$

and a solution $(\boldsymbol{u}_h,p_h,\theta_h)\colon [0,T]\to \boldsymbol{V}_h^{div}\times Q_h\times\Theta_h$ *of (7)-(8) satisfying* $\boldsymbol{u}_h\in L^\infty(0,T;[L^\infty(\Omega)]^d)$. *Let Assumptions 1 – 4 be valid as well as* $\boldsymbol{u}_h(0)=j_u\boldsymbol{u}_0$, $\theta_h(0)=j_\theta\theta_0$ *hold. For* $0\le t\le T$, *we obtain the estimate for the semi-discrete error* $\boldsymbol{\xi}_{u,h}=\boldsymbol{u}-\boldsymbol{u}_h$, $\xi_{\theta,h}=\theta-\theta_h$*:*

$$\begin{aligned}&\|\boldsymbol{\xi}_{u,h}\|^2_{L^\infty(0,t;L^2(\Omega))}+\|\xi_{\theta,h}\|^2_{L^\infty(0,t;L^2(\Omega))}\\ &\quad+\int_0^t\Big(|||\boldsymbol{\xi}_{u,h}(\tau)|||^2_{LPS}+|[\xi_{\theta,h}(\tau)]|^2_{LPS}\Big)\,\mathrm{d}\tau\\ &\lesssim\int_0^t e^{C_{G,h}(\boldsymbol{u},\theta)(t-\tau)}\Bigg\{\sum_{M\in\mathcal{M}_h}h_M^{2(k_p+1)}\min\Big(\frac{d}{\nu},\frac{1}{\gamma_M}\Big)\|p(\tau)\|^2_{W^{k_p+1,2}(\omega_M)}\\ &\quad+\sum_{M\in\mathcal{M}_h}h_M^{2k_u}\Big[(1+\nu+\tau_M^u|\boldsymbol{u}_M|^2+\gamma_M d)\|\boldsymbol{u}(\tau)\|^2_{W^{k_u+1,2}(\omega_M)}\\ &\qquad\qquad+\|\partial_t\boldsymbol{u}(\tau)\|^2_{W^{k_u,2}(\omega_M)}+\tau_M^u|\boldsymbol{u}_M|^2h_M^{2(s_u-k_u)}\|\boldsymbol{u}(\tau)\|^2_{W^{s_u+1,2}(\omega_M)}\Big]\\ &\quad+\sum_{L\in\mathcal{L}_h}h_L^{2k_\theta}\Big[\|\partial_t\theta(\tau)\|^2_{W^{k_\theta,2}(\omega_L)}+\tau_L^\theta|\boldsymbol{u}_L|^2h_L^{2(s_\theta-k_\theta)}\|\theta(\tau)\|^2_{W^{s_\theta+1,2}(\omega_L)}\Big]\\ &\quad+\Big(1+h_L^2\beta\|\boldsymbol{g}\|_{\infty,L}+\alpha+\tau_L^\theta|\boldsymbol{u}_L|^2\Big)\|\theta(\tau)\|^2_{W^{k_\theta+1,2}(\omega_L)}\Bigg\}\,\mathrm{d}\tau\end{aligned}\tag{24}$$

with $s_u\in\{0,\cdots,k_u\}$, $s_\theta\in\{0,\cdots,k_\theta\}$ *and a Gronwall constant as defined in Theorem 2.*

Proof We split the semi-discrete error as

$$\boldsymbol{\xi}_{u,h}=\boldsymbol{\eta}_{u,h}+\boldsymbol{e}_{u,h},\quad \xi_{\theta,h}=\eta_{\theta,h}+e_{\theta,h},\quad \xi_{p,h}=\eta_{p,h}+e_{p,h}$$

and use the triangle inequality in order to estimate the approximation and consistency errors separately. The interpolation results in $\boldsymbol{V}_h^{div}\times Q_h\times\Theta_h$, according to Assumption 1, are applied to Theorem 2. Further, we take advantage of the approximation properties of the fluctuation operators from Assumption 3 with $s_u\in\{0,\cdots,k_u\}$, $s_\theta\in\{0,\cdots,k_\theta\}$. This provides a bound for the consistency error in the following way for all $0\le\tau\le t\le T$

$$\begin{aligned}&\sum_{M\in\mathcal{M}_h}(\nu+\tau_M^u|\boldsymbol{u}_M|^2+d\gamma_M)\|\nabla\boldsymbol{\eta}_{u,h}(\tau)\|^2_{0,M}\\ &\quad+\sum_{M\in\mathcal{M}_h}h_M^{-2}\|\boldsymbol{\eta}_{u,h}(\tau)\|^2_{0,M}+\sum_{M\in\mathcal{M}_h}\min\Big(\frac{d}{\nu},\frac{1}{\gamma_M}\Big)\|\eta_{p,h}(\tau)\|^2_{0,M}\\ &\quad+\sum_{L\in\mathcal{L}_h}\left(\frac{1}{h_L^2}+\beta\|\boldsymbol{g}\|_{\infty,L}\right)\|\eta_{\theta,h}(\tau)\|^2_{0,L}+\big(\alpha+\tau_L^\theta|\boldsymbol{u}_L|^2\big)\|\nabla\eta_{\theta,h}(\tau)\|^2_{0,L}\end{aligned}$$

$$
\begin{aligned}
&\leq C \sum_{M\in\mathcal{M}_h} h_M^{2k_u}\Big(1+\tau_M^u|\boldsymbol{u}_M|^2+d\gamma_M\Big)\|\boldsymbol{u}(\tau)\|^2_{W^{k_u+1,2}(\omega_M)}\\
&\quad + C \sum_{M\in\mathcal{M}_h} h_M^{2(k_p+1)} \min\Big(\frac{d}{\nu},\frac{1}{\gamma_M}\Big)\|p(\tau)\|^2_{W^{k_p+1,2}(\omega_M)}\\
&\quad + \sum_{L\in\mathcal{L}_h} h_L^{2k_\theta}\left(1+h_L^2\beta\|\boldsymbol{g}\|_{\infty,L}+\alpha+\tau_L^\theta|\boldsymbol{u}_L|^2\right)\|\theta(\tau)\|^2_{W^{k_\theta+1,2}(\omega_L)}.
\end{aligned}
$$

Furthermore, it holds

$$
\begin{aligned}
\|\partial_t\boldsymbol{\eta}_{u,h}(\tau)\|_0^2 &\leq C\sum_{M\in\mathcal{M}_h} h_M^{2k_u}\|\partial_t\boldsymbol{u}(\tau)\|^2_{W^{k_u,2}(\omega_M)},\\
\tau_M^u|\boldsymbol{u}_M|^2\|\kappa_M^u(\nabla\boldsymbol{u}(\tau))\|^2_{0,M} &\leq C\sum_{M\in\mathcal{M}_h} \tau_M^u|\boldsymbol{u}_M|^2 h_M^{2s_u}\|\boldsymbol{u}\|^2_{W^{s_u+1,2}(\omega_M)},\\
\|\partial_t\eta_{\theta,h}(\tau)\|_0^2 &\leq C\sum_{L\in\mathcal{L}_h} h_L^{2k_\theta}\|\partial_t\theta(\tau)\|^2_{W^{k_\theta,2}(\omega_L)},\\
\tau_L^\theta|\boldsymbol{u}_L|^2\|\kappa_L^\theta(\nabla\theta(\tau))\|^2_{0,L} &\leq C\sum_{L\in\mathcal{L}_h} \tau_L^\theta|\boldsymbol{u}_L|^2 h_L^{2s_\theta}\|\theta(\tau)\|^2_{W^{s_\theta+1,2}(\omega_L)}.
\end{aligned}
$$

For the interpolation errors, we exploit the approximation properties from Assumption 1:

$$
\begin{aligned}
\|\boldsymbol{\eta}_{u,h}(\tau)\|_0^2 &\leq C\sum_{M\in\mathcal{M}_h} h_M^{2(k_u+1)}\|\boldsymbol{u}(\tau)\|^2_{W^{k_u+1,2}(\omega_M)},\\
\|\eta_{\theta,h}\|_0^2 &\leq C\sum_{L\in\mathcal{L}_h} h_L^{2(k_\theta+1)}\|\theta(\tau)\|^2_{W^{k_\theta+1,2}(\omega_L)},\\
|||\boldsymbol{\eta}_{u,h}(\tau)|||^2_{LPS} &\leq \sum_{M\in\mathcal{M}_h}\big(\nu+\tau_M^u|\boldsymbol{u}_M|^2+\gamma_M d\big)\|\nabla\boldsymbol{\eta}_{u,h}(\tau)\|^2_{0,M}\\
&\leq C\sum_{M\in\mathcal{M}_h} h_M^{2k_u}\big(\nu+\tau_M^u|\boldsymbol{u}_M|^2+\gamma_M d\big)\|\boldsymbol{u}(\tau)\|^2_{W^{k_u+1,2}(\omega_M)},\\
|[\eta_{\theta,h}(\tau)]|^2_{LPS} &\leq \sum_{L\in\mathcal{L}_h}\big(\alpha+\tau_L^\theta|\boldsymbol{u}_L|^2\big)\|\nabla\eta_{\theta,h}\|^2_{0,M}\\
&\leq C\sum_{L\in\mathcal{L}_h} h_L^{2k_\theta}\big(\alpha+\tau_L^\theta|\boldsymbol{u}_L|^2\big)\|\theta(\tau)\|^2_{W^{k_\theta+1,2}(\omega_L)}.
\end{aligned}
$$

The combination gives the claim.

Remark 2 Note that the above results do not provide a priori bounds since the Gronwall constant depends on $\|\boldsymbol{u}_h\|_\infty$. This allows us to prevent mesh width restrictions of the form

$$
Re_M=\frac{h_M\|\boldsymbol{u}_h\|_{\infty,M}}{\nu}\leq\frac{1}{\sqrt{\nu}},\qquad\qquad Pe_L=\frac{h_L\|\boldsymbol{u}_h\|_{\infty,L}}{\alpha}\leq\frac{1}{\sqrt{\alpha}},
$$

similar to the ones obtained in [8].

Remark 3 Provided a certain compatibility condition between fine and coarse ansatz spaces holds true (according to [5]), we can improve the above results similarly to the consideration in [8]. In particular, we obtain

$$
\begin{aligned}
&\|\boldsymbol{e}_{u,h}\|^2_{L^\infty(0,t;L^2(\Omega))} + \|e_{\theta,h}\|^2_{L^\infty(0,t;L^2(\Omega))} \\
&\quad + \int_0^t \Big(|||\boldsymbol{e}_{u,h}(\tau)|||^2_{LPS} + |[e_{\theta,h}(\tau)]|^2_{LPS} \Big)\, \mathrm{d}\tau \\
&\leq C \int_0^t e^{C'_{G,h}(\boldsymbol{u},\theta,\boldsymbol{u}_h)(t-\tau)} \Bigg\{ \sum_{M\in\mathcal{M}_h} \min\Big(\frac{d}{\nu}, \frac{1}{\gamma_M}\Big) \|\eta_{p,h}(\tau)\|^2_{0,M} \\
&\quad + \sum_{M\in\mathcal{M}_h} \Big[\big(\nu + \tau^u_M |\boldsymbol{u}_M|^2 + \gamma_M d\big) \|\nabla \boldsymbol{\eta}_{u,h}(\tau)\|^2_{0,M} + \Big(\frac{1}{h^2_M} + \frac{1}{\tau^u_M}\Big) \|\boldsymbol{\eta}_{u,h}(\tau)\|^2_{0,M} \\
&\qquad\qquad + \|\partial_t \boldsymbol{\eta}_{u,h}(\tau)\|^2_{0,M} + \tau^u_M |\boldsymbol{u}_M|^2 \|\kappa^u_M(\nabla \boldsymbol{u})(\tau)\|^2_{0,M} \Big] \\
&\quad + \sum_{L\in\mathcal{L}_h} \Big[\big(\alpha + \tau^\theta_L |\boldsymbol{u}_L|^2\big) \|\nabla \eta_{\theta,h}(\tau)\|^2_{0,L} + \Big(\frac{1}{\tau^\theta_L} + \beta \|\boldsymbol{g}\|_{\infty,L}\Big) \|\eta_{\theta,h}(\tau)\|^2_{0,L} \\
&\qquad\qquad + \tau^\theta_L |\boldsymbol{u}_L|^2 \|\kappa^\theta_L(\nabla\theta)(\tau)\|^2_{0,L} + \|\partial_t \eta_{\theta,h}(\tau)\|^2_{0,L} \Big] \Bigg\}\, \mathrm{d}\tau
\end{aligned}
$$

with Gronwall constant

$$
\begin{aligned}
C'_G(\boldsymbol{u},\theta,\boldsymbol{u}_h) = 1 &+ \beta\|\boldsymbol{g}\|_\infty + |\boldsymbol{u}|_{W^{1,\infty}(\Omega)} + |\theta|_{W^{1,\infty}(\Omega)} \\
&+ \max_{M\in\mathcal{M}_h} \{h^2_M |\boldsymbol{u}|^2_{W^{1,\infty}(M)}\} + \max_{M\in\mathcal{M}_h} \Big\{ \frac{h^2_M}{\gamma_M} |\boldsymbol{u}|^2_{W^{1,\infty}(M)} \Big\} \\
&+ \max_{M\in\mathcal{M}_h} \{\gamma^{-1}_M \|\boldsymbol{u}\|^2_{\infty,M}\} + \max_{M\in\mathcal{M}_h} \{h^2_M |\theta|^2_{W^{1,\infty}(M)}\} \\
&+ \max_{M\in\mathcal{M}_h} \Big\{ \frac{h^2_M}{\gamma_M} |\theta|^2_{W^{1,\infty}(M)} \Big\} + \max_{M\in\mathcal{M}_h} \{\gamma^{-1}_M \|\theta\|^2_{\infty,M}\} \\
&+ \max_{M\in\mathcal{M}_h} \Big\{ \tau^u_M |\boldsymbol{u}_h|^2_{W^{1,\infty}(M)} \Big\} + \max_{L\in\mathcal{L}_h} \Big\{ \tau^\theta_L |\boldsymbol{u}_h|^2_{W^{1,\infty}(L)} \Big\}.
\end{aligned}
$$

For more details, compare with [16].

Remark 4 From the above estimates, we can derive an error estimate for the pressure via the discrete inf-sup condition. If

$$
\boldsymbol{u} \in L^\infty(0,T;[W^{1,\infty}(\Omega)]^d), \quad \boldsymbol{u}_h \in L^\infty(0,T;[L^\infty(\Omega)]^d),
$$

we obtain the estimate for the semi-discrete pressure error $\xi_{p,h} = p - p_h$ for $0 \leq t \leq T$

$$
\begin{aligned}
&\|\xi_{p,h}\|^2_{L^2(0,t;L^2(\Omega))} \\
&\leq \frac{C}{\beta^2_d} \Bigg\{ \|\partial_t \boldsymbol{\xi}_{u,h}\|^2_{L^2(0,t;H^{-1}(\Omega))} + \beta^2 \|\boldsymbol{g}\|^2_{L^\infty(0,t;L^\infty(\Omega))} \|\xi_{\theta,h}\|^2_{L^2(0,t;L^2(\Omega))} \\
&\qquad + \big(\|\boldsymbol{u}\|^2_{L^2(0,t;L^\infty(\Omega))} + \|\boldsymbol{u}_h\|^2_{L^2(0,t;L^\infty(\Omega))} \big) \|\boldsymbol{\xi}_{u,h}\|^2_{L^\infty(0,t;L^2(\Omega))} \\
&\qquad + \int_0^t \Big(\nu + \max_{M\in\mathcal{M}_h} \{\gamma^{-1}_M \|\boldsymbol{u}_h\|^2_{\infty,M}\}
\end{aligned}
$$

$$+ \max_{M\in\mathcal{M}_h}\{\tau_M^u|\boldsymbol{u}_M|^2\} + \max_{M\in\mathcal{M}_h}\{\gamma_M d\}\Big)|||\boldsymbol{\xi}_{u,h}|||_{LPS}^2\,\mathrm{d}\tau$$
$$+ \int_0^t \max_{M\in\mathcal{M}_h}\{\tau_M^u|\boldsymbol{u}_M|^2\}\sum_{M\in\mathcal{M}_h}\tau_M^u|\boldsymbol{u}_M|^2\|\kappa_M^u(\nabla\boldsymbol{u})\|_{0,M}^2\mathrm{d}\tau\Bigg\}$$

with a constant $C > 0$ independent of the problem parameters, h_M, h_L and the solutions. We point out that the estimate is not optimal due to the term $\|\partial_t\boldsymbol{\xi}_{u,h}\|^2_{L^2(0,t;H^{-1}(\Omega))}$. In [9], an improved result for the Navier-Stokes equations is obtained.

4.3 Suitable Finite Element Spaces

We address the question of suitable settings for our analysis in Theorem 2 and Corollary 1. First, let us introduce some notation.

For a simplex $T \in \mathcal{T}_h$ or a quadrilateral/hexahedron T in $\mathbb{R}^d$, let $\hat{T}$ be the reference unit simplex or the unit cube $(-1,1)^d$. We are interested in so-called mapped finite elements, that are constructed as transformations from the reference element. Denote by $F_T\colon \hat{T} \to T$ the reference mapping. For simplices T, F_T is affine and bijective. In case of quadrilaterals/hexahedra, F_T is a multi-linear mapping from $\hat{T}$ to arbitrary quadrilaterals/hexahedra. Henceforth, we require that F_T is bijective and its Jacobian is bounded for a family of triangulations according to

$$\exists\, c_1,\, c_2 > 0\colon \quad c_1 h_T^d \le |\det DF_T(\hat{\boldsymbol{x}})| \le c_2 h_T^d \quad \forall\,\hat{\boldsymbol{x}} \in \hat{T} \tag{25}$$

with constants c_1, $c_2 > 0$ independent of the cell diameter h_T.

Let $\hat{\mathbb{P}}_l$ and $\hat{\mathbb{Q}}_l$ with $l \in \mathbb{N}_0$ be the set of polynomials of degree $\le l$ and of polynomials of degree $\le l$ in each variable separately. Moreover, we set

$$\mathbb{R}_l(\hat{T}) := \begin{cases} \mathbb{P}_l(\hat{T}) & \text{on simplices } \hat{T} \\ \mathbb{Q}_l(\hat{T}) & \text{on quadrilaterals/hexahedra } \hat{T}. \end{cases}$$

Bubble-enriched spaces are

$$\mathbb{P}_l^+(\hat{T}) := \mathbb{P}_l(\hat{T}) + b_{\hat{T}}\cdot\mathbb{P}_{l-2}(\hat{T}), \quad \mathbb{Q}_l^+(\hat{T}) := \mathbb{Q}_l(\hat{T}) + \psi\cdot\mathrm{span}\{\hat{x}_i^{r-1},\, i = 1,\dots,d\}$$

with polynomial bubble function $b_{\hat{T}} := \prod_{i=0}^d \hat{\lambda}_i \in \hat{\mathbb{P}}_{d+1}$ on the reference simplex $\hat{T}$ with barycentric coordinates $\hat{\lambda}_i$ and with d-quadratic function $\psi(\hat{x}) := \prod_{i=1}^d(1-\hat{x}_i^2)$ on the reference cube. Define

$$Y_{h,-l} := \{v_h \in L^2(\Omega) :\ v_h|_T \circ F_T \in \mathbb{R}_l(\hat{T})\ \forall T \in \mathcal{T}_h\},$$
$$Y_{h,l} := Y_{h,-l} \cap W^{1,2}(\Omega)$$

and bubble-enriched spaces $Y^+_{h,\pm l}$, analogously. For convenience, we write $\boldsymbol{V}_h = \mathbb{R}_k$ instead of $\boldsymbol{V}_h := [Y_{h,k}]^d \cap V$ for the velocity (with obvious modifications for $\mathbb{R}_k^+$) and similarly for pressure and temperature.

The presented approach is applicable to many combinations of ansatz spaces. The interpolation property from Assumption 1 and the discrete inf-sup condition (4) hold for our finite element setting of Lagrangian elements

$$\boldsymbol{V}_h = \mathbb{R}^{(+)}_{k_u}, \qquad Q_h = \mathbb{R}_{\pm(k_u-1)}, \qquad \Theta_h = \mathbb{R}^{(+)}_{k_\Theta}$$

with $k_u \geq 2$, $k_\theta \geq 2$. It is shown in [15] that there exists a quasi-local interpolation operator that preserves the discrete divergence and has the needed approximation properties in Assumption 1 on simplicial isotropic meshes. It is argued in [15] that the result can be easily extended to quadrilateral/hexahedral meshes and in this case to $k_u = 2, d = 3$.

In [6] (Table 1 and 2), fine and coarse discrete ansatz spaces are presented that fulfill the approximation property of the fluctuation operators (Assumption 3). We summarize possible variants of the triples $(\boldsymbol{V}_h/\boldsymbol{D}^u_M) \wedge Q_h \wedge (\Theta_h/D^\theta_L)$ with $s_u \in \{1,\dots,k_u\}$, $s_\theta \in \{1,\dots,k_\theta\}$.

- One-level methods:
  $(\mathbb{P}_{k_u}/\mathbb{P}_{s_u-1}) \wedge \mathbb{P}_{k_u-1} \wedge (\mathbb{P}_{k_\theta}/\mathbb{P}_{s_\theta-1})$, $(\mathbb{Q}_{k_u}/\mathbb{Q}_{s_u-1}) \wedge \mathbb{Q}_{k_u-1} \wedge (\mathbb{Q}_{k_\theta}/\mathbb{Q}_{s_\theta-1})$,
  $(\mathbb{P}^+_{k_u}/\mathbb{P}_{s_u-1}) \wedge \mathbb{P}_{-(k_u-1)} \wedge (\mathbb{P}^+_{k_\theta}/\mathbb{P}_{s_\theta-1})$, $(\mathbb{Q}_{k_u}/\mathbb{P}_{s_u-1}) \wedge \mathbb{P}_{-(k_u-1)} \wedge (\mathbb{Q}_{k_\theta}/\mathbb{P}_{s_\theta-1})$.
- Two-level methods (for the construction of the coarse space, see [5,6]):
  $(\mathbb{P}_{k_u}/\mathbb{P}_{s_u-1}) \wedge \mathbb{P}_{k_u-1} \wedge (\mathbb{P}_{k_\theta}/\mathbb{P}_{s_\theta-1})$, $(\mathbb{Q}_{k_u}/\mathbb{Q}_{s_u-1}) \wedge \mathbb{Q}_{k_u-1} \wedge (\mathbb{Q}_{k_\theta}/\mathbb{Q}_{s_\theta-1})$,
  $(\mathbb{P}^+_{k_u}/\mathbb{P}_{s_u-1}) \wedge \mathbb{P}_{-(k_u-1)} \wedge (\mathbb{P}^+_{k_\theta}/\mathbb{P}_{s_\theta-1})$, $(\mathbb{Q}_{k_u}/\mathbb{P}_{s_u-1}) \wedge \mathbb{P}_{-(k_u-1)} \wedge (\mathbb{Q}_{k_\theta}/\mathbb{P}_{s_\theta-1})$.

4.4 Parameter Choice

The presented possibilities of finite element combinations result in a parameter choice as

$$\gamma_M = \gamma_0, \quad 0 \leq \tau^u_M(\boldsymbol{u}_M) \leq \tau^u_0 \frac{h_M^{2(k_u-s_u)}}{|\boldsymbol{u}_M|^2}, \quad 0 \leq \tau^\theta_L(\boldsymbol{u}_L) \leq \tau^\theta_0 \frac{h_L^{2(k_\theta-s_\theta)}}{|\boldsymbol{u}_L|^2} \tag{26}$$

for $M \in \mathcal{M}_h$ and $L \in \mathcal{L}_h$, where $\gamma_0, \tau^u_0, \tau^\theta_0 = \mathcal{O}(1)$ denote non-negative tuning constants. With the parameter choice (26), Assumption 4 is satisfied. In these possible settings, we can apply Theorem 2 and Corollary 1. We point out that in order to get an optimal rate k in (24), one might want to choose

$$k := k_u = k_\theta = k_p + 1.$$

A choice of grad-div and LPS SU parameters as in (26) balances the terms in the upper bound of the semi-discrete error (24). In addition, the Gronwall constant (19) does not blow up for small ν if $\gamma_M > 0$. An h-independent γ_M (or at least $\gamma_M \geq Ch$) also diminishes the growth of the Gronwall constant with $|\boldsymbol{u}|_{W^{1,\infty}(\Omega)}$ and $|\theta|_{W^{1,\infty}(\Omega)}$ and is therefore favorable. In case of $\boldsymbol{u}_M = \boldsymbol{0}$, we set $\tau^u_M(\boldsymbol{u}_M) = 0$ and $\tau^\theta_L(\boldsymbol{u}_L) = 0$ if $\boldsymbol{u}_L = \boldsymbol{0}$ as the whole LPS terms vanish. In [6], similar bounds for the Oseen problem are proposed: $\tau^u_M |\boldsymbol{b}_M|^2 \leq C h_M^{k-s_u}$ and $\gamma_M \sim 1$.
Comparing the physical dimensions in the momentum equation (7) and the Fourier equation (8), we obtain

$$[\tau^u_M(\boldsymbol{u}_M)]\,\frac{m^2}{s^4} = [s_u(\boldsymbol{u}_h;\boldsymbol{u}_h,\boldsymbol{u}_h)] = \left[\left(\frac{\partial \boldsymbol{u}_h}{\partial t}, \boldsymbol{u}_h\right)\right] = \frac{m^2}{s^3}$$

$$\left[\tau_L^\theta(\boldsymbol{u}_L)\right]\frac{K^2}{s^2} = [s_\theta(\boldsymbol{u}_h;\theta_h,\theta_h)] = \left[\left(\frac{\partial\theta_h}{\partial t},\theta_h\right)\right] = \frac{K^2}{s}.$$

This suggests a parameter design as

$$\tau_L^\theta(\boldsymbol{u}_L) \sim h_L/|\boldsymbol{u}_L|, \quad \tau_M^u(\boldsymbol{u}_M) \sim h_M/|\boldsymbol{u}_M|, \tag{27}$$

that is within the above (theoretical) parameter bounds. We will consider this choice in the numerical examples.
The design of the grad-div parameter set $\{\gamma_M\}_M$ is still an open problem, see e.g. [17] for the Stokes problem. An equilibration argument in our analysis (24) suggests

$$\gamma_M \sim \max\left(0; \frac{\|p\|_{W^{k,2}(M)}}{\|\boldsymbol{u}\|_{W^{k+1,2}(M)}} - \nu\right). \tag{28}$$

Indeed, in different flow examples, the choice (28) yields distinct γ_M: In case of flow with $\boldsymbol{f}_u \equiv \boldsymbol{0}$, $(\boldsymbol{u}\cdot\nabla)\boldsymbol{u} = \partial_t\boldsymbol{u} = \boldsymbol{0}$ and $-\nu\Delta\boldsymbol{u} + \nabla p = \boldsymbol{0}$ (Poiseuille flow), we would choose $\gamma_M = 0$, as $\|p\|_{W^{k,2}(\Omega)}/\|\boldsymbol{u}\|_{W^{k+1,2}(\Omega)} \sim \nu$. For the Taylor-Green vortex with $\boldsymbol{f}_u \equiv \boldsymbol{0}$, one has $\partial_t\boldsymbol{u} - \nu\Delta\boldsymbol{u} = \boldsymbol{0}$ and $(\boldsymbol{u}\cdot\nabla)\boldsymbol{u} + \nabla p = 0$, thus leading to $\|p\|_{W^{k,2}(\Omega)}/\|\boldsymbol{u}\|_{W^{k+1,2}(\Omega)} \sim 1$. If ν is small, $\gamma_M \sim 1$ follows. Unfortunately, (28) is not a viable choice for γ_M in practice.
Especially in the advection dominated case, grad-div stabilization with $\gamma_M > \nu$ has a regularizing effect. Furthermore, $\gamma_M > \nu$ is essential for the independence of the Gronwall constant $C_{G,h}(\boldsymbol{u},\theta)$ of ν. Corollary 1 and the above discussion clarify that $\gamma_M = \mathcal{O}(1)$ is a reasonable compromise. Our numerical tests also confirm this.

5 Numerical Examples

In order to validate the analytical results, we need to discretize the semi-discrete formulation in time as well. The method we choose is a splitting method called rotational pressure-correction projection method, which is based on the backward differentiation formula of second order (BDF2). This method has been proposed by Timmermans [18] for the Navier-Stokes case and has been analyzed for the linear Stokes model in [19].
With the constant time step size $\Delta t > 0$, the scheme reads:

Find $\boldsymbol{u}_{ht}^n \in \boldsymbol{V}_h$ such that for all $\boldsymbol{v}_h \in \boldsymbol{V}_h$:

$$\begin{aligned}&\left(\frac{3\boldsymbol{u}_{ht}^n - 4\boldsymbol{u}_{ht}^{n-1} + \boldsymbol{u}_{ht}^{n-2}}{2\Delta t}, \boldsymbol{v}_h\right) + \nu(\nabla\boldsymbol{u}_{ht}^n, \nabla\boldsymbol{v}_h) + c_u(\boldsymbol{u}_{ht}^n;\boldsymbol{u}_{ht}^n,\boldsymbol{v}_h)\\ &\quad + t_h(\boldsymbol{u}_{ht}^n;\boldsymbol{u}_{ht}^n,\boldsymbol{v}_h) + s_u(\boldsymbol{u}_{ht}^n;\boldsymbol{u}_{ht}^n,\boldsymbol{v}_h) - (p_{ht}^{n-1}, \nabla\cdot\boldsymbol{v}_h) + \beta(\boldsymbol{g}(t_n)\theta_{ht}^{n*}, \boldsymbol{v}_h)\\ &= (\boldsymbol{f}_u(t_n), \boldsymbol{v}_h) + \left(\frac{7}{3}p_{ht}^{n-1} - \frac{5}{3}p_{ht}^{n-2} + \frac{1}{3}p_{ht}^{n-3}, \nabla\cdot\boldsymbol{v}_h\right),\end{aligned} \tag{29}$$

where $\theta_{ht}^{n*} := 2\theta_{ht}^{n-1} - \theta_{ht}^{n-2}$ is an extrapolation of second order of the temperature θ_{ht}^n.

Find $q_{ht}^n \in Q_h$ such that for all $q_h \in Q_h$:

$$(\nabla(p_{ht}^n - p_{ht}^{n-1}), \nabla q_h) = \left(\frac{3\nabla\cdot\boldsymbol{u}_{ht}^n}{2\Delta t}, q_h\right). \tag{30}$$

Find $\theta_{ht}^n \in \Theta_h$ such that for all $\psi_h \in \Theta_h$:

$$\begin{aligned}&\left(\frac{3\theta_{ht}^n - 4\theta_{ht}^{n-1} + \theta_{ht}^{n-2}}{2\Delta t}, \psi_h\right) + \alpha(\nabla\theta_{ht}^n, \nabla\psi_h)\\ &\quad + c_\theta(\boldsymbol{u}_{ht}^n; \theta_{ht}^n, \psi_h) + s_\theta(\boldsymbol{u}_{ht}^n; \theta_{ht}^n, \psi_h)\\ &= (f_\theta(t_n), \psi_h).\end{aligned} \tag{31}$$

Using this scheme, we want to confirm the results obtained above numerically and investigate suitable parameter choices for the stabilizations. Therefore, we first consider an artificial example using the method of manufactured solution. Due to the fact that we know the analytical solution, we can observe in which cases we obtain the desired rates of convergence. In the second example, we consider Rayleigh-Bénard convection in a cylinder. This problem is well-investigated and we consider the influence of stabilization on typical benchmark quantities.

Remark 5 For the fully discrete quantities, one can show stability according to

$$\begin{aligned}&\|\boldsymbol{u}_{ht}\|^2_{l^\infty(0,T;L^2(\Omega))} + \|\boldsymbol{u}_{ht}\|^2_{l^2(0,T;LPS)} + (\Delta t)^2\|\nabla p_{ht}\|^2_{l^\infty(0,T;L^2(\Omega))}\\ &\quad + \|\theta_{ht}\|^2_{l^\infty(0,T;L^2(\Omega))} + \|\theta_{ht}\|^2_{l^2(0,T;LPS)}\\ &\leq C(\boldsymbol{u}_{ht}^0, \boldsymbol{u}_{ht}^1, p_{ht}^0, p_{ht}^1, \theta_{ht}^0, \theta_{ht}^1, \beta, \boldsymbol{g}, \boldsymbol{f}_u, f_\theta),\end{aligned}$$

cf. [16]. We expect that the convergence results for the stabilized Navier-Stokes in [20] can be extended to the Oberbeck-Boussinesq model easily due to the similarity of the momentum and the Fourier equations and their weak coupling.

5.1 Traveling Wave

We consider a time dependent, two-dimensional solution of the Oberbeck-Boussinesq equations (1) for different parameters $\nu, \alpha, \beta > 0$ in a box $\Omega = (0,1)^2$ with $t \in [0, 6 \cdot 10^{-3}]$:

$$\begin{aligned}&\boldsymbol{u}(x,y,t) = (100, 0)^T, \quad p(x,y,t) = 0,\\ &\theta(x,y,t) = (1 + 3200\alpha t)^{-1/2} \exp\left(-\left(\frac{1}{2} + 100tx\right)^2 \left(\frac{1}{800} + 4\alpha t\right)^{-1}\right)\end{aligned}$$

with $\boldsymbol{g} \equiv (0, -1)^T$ and (time dependent) Dirichlet boundary conditions for $\boldsymbol{u}$ and θ. The right-hand sides $\boldsymbol{f}_u$, f_θ are calculated such that $(\boldsymbol{u}, p, \theta)$ solves the equations. Initially, the temperature peak is located at $x = \frac{1}{2}$ and moves in x-direction until it finally hits the wall at $x = 1, t = 0.005$ and is transported out of the domain. Note that the movement of the peak is one-dimensional.

The mesh is randomly distorted by 1%; h denotes an average cell diameter. We use $\mathbb{Q}_2 \wedge \mathbb{Q}_1 \wedge (\mathbb{Q}_2/\mathbb{Q}_1)$ or $\mathbb{Q}_2 \wedge \mathbb{Q}_1 \wedge (\mathbb{Q}_2^+/\mathbb{Q}_1)$ elements for velocity, pressure and fine and coarse temperature. Since only the temperature ansatz spaces are varied here, we write $\mathbb{Q}_2^{(+)}/\mathbb{Q}_1$ for convenience.

As presented in Figure 1, we obtain the expected order of convergence for the LPS-error $|||\boldsymbol{u} - \boldsymbol{u}_h|||_{LPS} + |[\theta - \theta_h]|_{LPS} \sim h^2$ even without stabilization. Adding LPS stabilization for θ does not corrupt this result. Note that even a high

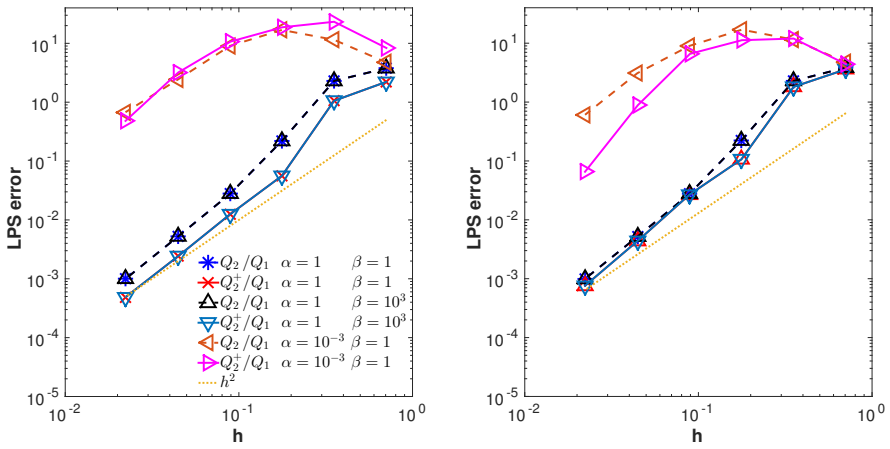

(a) (b)

Fig. 1: LPS-errors for different finite elements and choices of α and β with (a) $\tau_L^\theta = 0$ and (b) $\tau_L^\theta = h/\|\boldsymbol{u}_h\|_{\infty,L}$, $\nu = 1$

parameter β does not require any stabilization: Neither the discrete temperature nor velocity or pressure fail to converge properly (not shown). In the interesting case $\alpha = 10^{-3}$, the LPS-errors become very large in the unstabilized case. LPS stabilization in combination with $\mathbb{Q}_2^+/\mathbb{Q}_1$ elements for θ_h cures this situation (Figure 1 (b)).

In the unstabilized case as well as in case of LPS SU with $\mathbb{Q}_2/\mathbb{Q}_1$ elements for the temperature, the spurious oscillations of the discrete temperature cannot be captured. These wiggles are directly visible in Figure 2, where $\theta_h(x, y = 0.5, t = 0.005)$ is plotted for $x \in [0, 0.9]$. The improvement becomes obvious if we use enriched elements $\mathbb{Q}_2^+/\mathbb{Q}_1$.

5.2 Rayleigh-Bénard convection

We consider Rayleigh-Bénard convection in a three-dimensional cylindrical domain

$$\Omega := \left\{ (x, y, z) \in \left(-\frac{1}{2}, \frac{1}{2}\right)^3 \,\middle|\, \sqrt{x^2 + y^2} \leq \frac{1}{2},\ |z| \leq \frac{1}{2} \right\}$$

with aspect ratio $\Gamma = 1$ for Prandtl number $Pr = 0.786$ and different Rayleigh numbers $10^5 \leq Ra \leq 10^9$. These critical parameters are defined by

$$Pr = \frac{\nu}{\alpha} \quad Ra = \frac{|\boldsymbol{g}|\beta\Delta\theta_{\text{ref}} L_{\text{ref}}^3}{\nu\alpha}.$$

In this testcase the gravitational acceleration $\boldsymbol{g} \equiv (0, 0, -1)^T$ is (anti-)parallel to the z-axis. The temperature is fixed by Dirichlet boundary conditions at the (warm) bottom and (cold) top plate; the vertical wall is adiabatic with Neumann

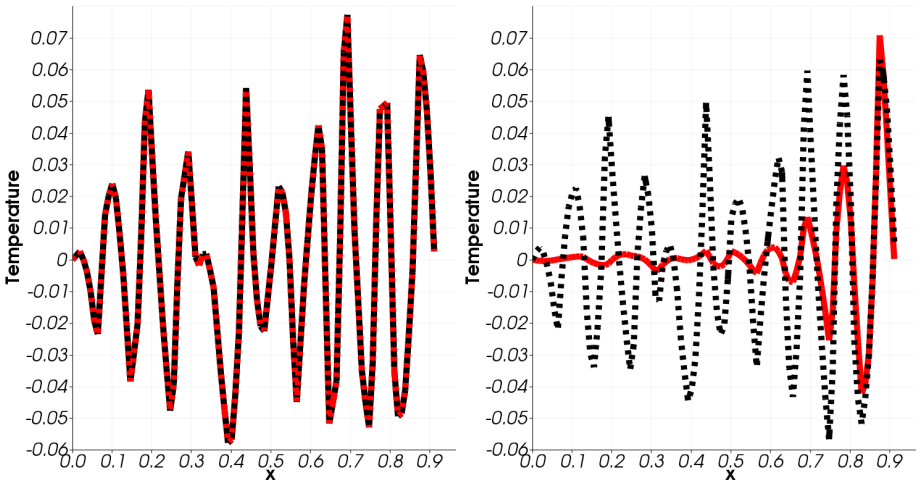

(a) (b)

Fig. 2: Plot over temperature at $y = 0.5$ ($x \in [0, 0.9]$) at time $t = 0.005$ with $h = 1/16$ in case of (a) $\mathbb{Q}_2/\mathbb{Q}_1$ elements for $\tau_L^\theta = 0$ (dotted line and for $\tau_L^\theta = \|\boldsymbol{u}_h\|_{\infty,L}^{-2}$ (solid line), (b) $\mathbb{Q}_2^+/\mathbb{Q}_1$ elements for $\tau_L^\theta = 0$ (dotted line) and for $\tau_L^\theta = \|\boldsymbol{u}_h\|_{\infty,L}^{-2}$ (solid line), $(\nu, \alpha, \beta) = (1, 10^{-3}, 1)$. The dotted and solid lines lie on top of each other in (a)

boundary conditions $\frac{\partial\theta}{\partial \boldsymbol{n}} = 0$. Homogeneous Dirichlet boundary data for the velocity are prescribed. We use triangulations with N cells, where $N \in \{10 \cdot 8^3, 10 \cdot 16^3, 10 \cdot 32^3\}$, as well as a time step size $\Delta t = 0.1$ for $N = 10 \cdot 8^3$, $\Delta t = 0.05$ for $N = 10 \cdot 16^3$ and $\Delta t = 0.01$ for $N = 10 \cdot 32^3$.

As a benchmark quantity, the Nusselt number Nu is used. With $B := \{(x, y) \in (-\frac{1}{2}, \frac{1}{2})^2 \mid \sqrt{x^2 + y^2} \leq \frac{1}{2}\}$, the Nusselt number Nu at fixed z is calculated from the vertical heat flux $q_z = u_z\theta - \alpha\frac{\partial\theta}{\partial z}$ from the warm wall to the cold one by averaging over B and in time:

$$Nu(z) = \Gamma\Big(\alpha|B|(T - t_0)\,|\theta_{bottom} - \theta_{top}|\Big)^{-1} \int_{t_0}^{T}\int_B q_z(x, y, z, t)\,dx\,dy\,dt$$

with a suitable interval $[t_0, T]$. It is well known that the time averaged Nusselt number does not depend on z. In order to assess the quality of our simulations, we compute the Nusselt number for different $z \in \{-0.5, -0.25, 0, 0.25, 0.5\}$, where the heat transfer is integrated over a disk at fixed z. Then we compare these quantities with the Nusselt number Nu^{avg} calculated as the heat transfer averaged over the whole cylinder Ω and in time. The maximal deviation σ within the domain is evaluated according to

$$\sigma := \max\{|Nu^{\mathrm{avg}} - Nu(z)|,\ z \in \{-0.5, -0.25, 0, 0.25, 0.5\}\}.$$

For comparison, we consider the DNS simulations by [21] and denote the respective values by Nu^{ref}.

For high Rayleigh numbers, boundary layers occur in this test case. In order to resolve these layers in the numerical solution, the (isotropic) grid is transformed via $T_{xyz}\colon \Omega \to \Omega$ of the form

$$T_{xyz}\colon (x,y,z)^T \mapsto \left(\frac{x}{r} \cdot \frac{\tanh(4r)}{2\tanh(2)}, \frac{y}{r} \cdot \frac{\tanh(4r)}{2\tanh(2)}, \frac{\tanh(4z)}{2\tanh(2)} \right)^T \tag{32}$$

with $r := \sqrt{x^2+y^2}$.

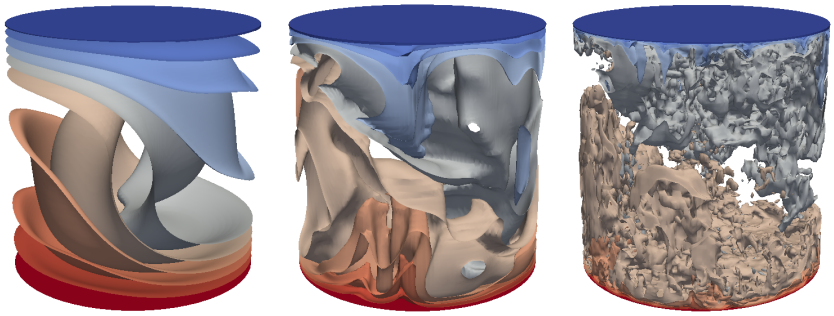

(a) (b) (c)

Fig. 3: Temperature iso-surfaces at $T = 1000$ for $Pr = 0.786$, (a) $Ra = 10^5$, (b) $Ra = 10^7$, (c) $Ra = 10^9$, $N = 10 \cdot 16^3$, $\gamma_M = 0.1$

A snapshot of temperature iso-surfaces for different Ra at $T = 1000$ is shown in Figure 3. $N = 10 \cdot 16^3$ cells, grad-div stabilization with $\gamma_M = 0.1$ and $\mathbb{Q}_2 \wedge \mathbb{Q}_1 \wedge \mathbb{Q}_2$ elements for velocity, pressure and temperature are used. Whereas the large scale behavior shows one large convection cell (upflow of warm fluid and descent of cold fluid) in all cases in a similar fashion, with larger Ra, smaller structures and thin boundary layers occur. For $Ra = 10^5$, the flow reaches a steady state, whereas $Ra \in \{10^7, 10^9\}$ results in transient flow. This is in good qualitative agreement with simulations run by [21].

First, we want to determine the optimal grad-div parameters depending on Ra. The resulting benchmark quantities without any stabilization and with optimal grad-div parameter are presented in Table 1; results for different grad-div parameters can be found in [16]. Only for $Ra = 10^5$, the unstabilized case $\gamma_M = 0$ gives satisfactory values for Nu^{avg} and σ; the discrepancy from Nu^{ref} is only 0.25%. Addition of grad-div stabilization does not corrupt this result. For higher Rayleigh numbers, $\gamma_M = 0$ leads to Nusselt numbers strongly depending on z and differing from the reference value by a large amount, for example by more than 88% of the absolute value Nu^{ref} in case of $Ra = 10^9$. Even negative Nusselt numbers occur for some z. Increasing the stabilization parameter to $\gamma_M = 0.01$ can reduce these differences to 12% for $Ra = 10^9$. Also, the deviation within the domain can be diminished considerably for all $Ra > 10^5$. The optimal grad-div parameter found by these experiments lies in the range $\gamma_M \in [0.01, 0.1]$ for all considered Rayleigh numbers. We infer that this parameter can be chosen independently from Ra.

Ra	10^5		10^6		10^7		10^8		10^9	
	Nu^{avg}	σ	Nu^{avg}	σ	Nu^{avg}	σ	Nu^{avg}	σ	Nu^{avg}	σ
nGD	3.84	0.04	8.65	0.34	16.41	1.83	37.70	29.5	118.8	137.6
GD	3.84	0.03	8.65	0.02	16.88	0.11	31.29	0.70	55.52	1.35
Nu^{ref}	3.83		8.6		16.9		31.9		63.1	

Table 1: Averaged Nusselt numbers and maximal deviations σ for different Ra and different grad-div parameters γ_M, averaged over time $t \in [150, 1000]$, $N = 10 \cdot 8^3$, $\mathbb{Q}_2 \wedge \mathbb{Q}_1 \wedge \mathbb{Q}_1$ elements are used. nGD indicates that no stabilization is used (in particular, $\gamma_M = 0$), GD means that an optimal grad-div parameter is used: $\gamma_M = 0.1$ for $10^5 \leq Ra \leq 10^8$ and $\gamma_M = 0.01$ for $Ra = 10^9$. Nu^{ref} denotes DNS results from [21]

Anyway, for all $Ra \in \{10^5, 10^6, 10^7, 10^8\}$, the reference values Nu^{ref} obtained by DNS can be approximated surprisingly well with the help of grad-div stabilization on a mesh with only $N = 10 \cdot 8^3$ cells. Also, the Nusselt number varies little with respect to different z.

τ_M^u	τ_L^θ	Nu_{th}^{avg}	σ_{th}	Nu_{bb}^{avg}	σ_{bb}	$Nu_{Id,th}^{\text{avg}}$	$\sigma_{Id,th}$	$Nu_{Id,bb}^{\text{avg}}$	$\sigma_{Id,bb}$
0	0	55.52	1.35	58.14	1.48	41.46	40.20	47.53	23.40
hu1	0	53.84	1.41	58.27	1.47	38.71	43.03	44.30	24.79
0	hu1	52.45	3.48	56.53	3.06	37.61	10.84	54.26	16.53
hu1	hu1	51.81	3.43	54.04	3.33	37.05	10.31	49.13	12.92

Table 2: Averaged Nusselt numbers and maximal deviations σ for different choices of stabilization and finite element spaces, $Ra = 10^9$, averaged over time $t \in [150, 1000]$, $N = 10 \cdot 8^3$. The subscript Id means that an isotropic grid is used; otherwise, the grid is transformed via T_{xyz}. The additional th indicates that $(\mathbb{Q}_2/\mathbb{Q}_1) \wedge \mathbb{Q}_1 \wedge (\mathbb{Q}_2/\mathbb{Q}_1)$ elements are used and $(\mathbb{Q}_2^+/\mathbb{Q}_1) \wedge \mathbb{Q}_1 \wedge (\mathbb{Q}_2^+/\mathbb{Q}_1)$ are denoted by bb. The label hu1 indicates that $\tau_{M/L}^{u/\theta} = \frac{1}{2} h / \|\boldsymbol{u}_h\|_{\infty, M/L}$. Nu^{ref} denotes DNS results from [21]

In order to examine the influence of additional LPS SU and different grids, we give an overview for different parameters with $(\mathbb{Q}_2/\mathbb{Q}_1) \wedge \mathbb{Q}_1 \wedge (\mathbb{Q}_2/\mathbb{Q}_1)$, indicated by th, and enriched $(\mathbb{Q}_2^+/\mathbb{Q}_1) \wedge \mathbb{Q}_1 \wedge (\mathbb{Q}_2^+/\mathbb{Q}_1)$ finite elements, denoted by bb, in Table 2; $Ra = 10^9$ and the optimal grad-div parameter $\gamma_M = 0.01$ are used. Note that the Nusselt numbers calculated with enriched elements are in better agreement with the reference value $Nu^{\text{ref}} = 63.1$ than using $(\mathbb{Q}_2/\mathbb{Q}_1) \wedge \mathbb{Q}_1 \wedge (\mathbb{Q}_2/\mathbb{Q}_1)$ elements. Our simulations support the conclusion that additional LPS SU stabilization is not needed in case of anisotropic grids that are adapted to the specific problem; grad-div suffices and is even more favorable. Stabilization of the velocity as $\tau_M^u \sim h/\|\boldsymbol{u}_h\|_{\infty, M}$ performs better than other LPS SU variants (see [16] for the results for more parameters). We also test an isotropic and globally refined grid, which is not particularly refined in boundary layer regions. In Table 2, the subscript Id indicates this grid. In general, the calculated benchmarks differ from the reference value Nu^{ref} by a larger amount than the ones obtained on a

grid that is refined within the boundary layer, even with the same number of cells. However, in case of an isotropic grid, the deviation is very large if grad-div stabilization is used solely; LPS SU stabilization becomes relevant: Since small temperature structures in the boundary layer are not resolved, their influence has to be modeled. Additional stabilization for the temperature serves this purpose. For instance, in case of $(\mathbb{Q}_2/\mathbb{Q}_1) \wedge \mathbb{Q}_1 \wedge (\mathbb{Q}_2/\mathbb{Q}_1)$ elements, it reduces $\sigma_{Id,th}$ from nearly 97% of the absolute value of the calculated Nusselt number $Nu^{\text{avg}}_{Id,th}$ in case of $(\gamma_M, \tau^u_M, \tau^\theta_L) = (0.01, 0, 0)$ to less than 30% if $\tau^\theta_L = \frac{1}{2}h/\|\boldsymbol{u}_h\|_{\infty,L}$. The use of enriched elements improves the results; a Nusselt number $Nu^{\text{avg}}_{Id,bb} = 54.2603$ is reached for $(\gamma_M, \tau^u_M, \tau^\theta_L) = (0.01, 0, \frac{1}{2}h/\|\boldsymbol{u}_h\|_{\infty,L})$.

Further, we try to improve the results for $Ra = 10^9$ by using finer grids with $N = 10 \cdot 16^3$ cells (with $\Delta t = 0.05$) and $N = 10 \cdot 32^3$ cells (with $\Delta t = 0.01$). The results are shown in Table 3. We first observe that adding LPS stabilization of any kind decreases the Nusselt number; we achieve best results on the grid with $N = 10 \cdot 16^3$ cells for grad-div stabilization alone. The obtained values still are too small by 4.1% for Taylor-Hood elements and by 2.8% for enriched elements. On the finest mesh, the Nusselt number still differs from Nu^{ref} by 1.5% if a grid transformed via T_{xyz} is used. We suppose that we can improve the results by adding more degrees of freedom in the middle of the domain by transforming the mesh in z-direction alone via $T_z \colon \Omega \to \Omega$ of the form

$$T_z \colon (x, y, z)^T \mapsto \left(x, y, \frac{\tanh(4z)}{2\tanh(2)}\right)^T \tag{33}$$

with $r := \sqrt{x^2 + y^2}$. The results for Nu^{avg} are best if additional LPS stabilization of the velocity is used and we get as close as 0.1% to the reference value. With grad-div stabilization alone, the Nusselt number differs from the reference value by 0.7%. This supports the expectation that for the Nusselt number, resolving boundary layers at the top and bottom is more important than at the hull.

N			γ_M	τ^u_M	τ^θ_L	Nu^{avg}	σ	Nu^{ref}
$10 \cdot 16^3$	*th*	T_{xyz}	0.01	0	0	60.49	1.16	63.1
	th	T_{xyz}	0.01	hu1	0	59.16	1.27	
	th	T_{xyz}	0.01	0	hu1	59.67	0.98	
	th	T_{xyz}	0.01	hu1	hu1	58.72	1.23	
	bb	T_{xyz}	0.01	0	0	61.34	0.54	
$10 \cdot 32^3$	*th*	T_{xyz}	0.01	0	0	62.14	0.68	
	th	T_z	0.01	0	0	62.65	0.55	
	th	T_z	0.01	hu1	0	63.01	0.78	
	th	T_z	0.01	0	hu1	62.47	0.54	

Table 3: Averaged Nusselt numbers and maximal deviations σ for different grids and choices of stabilization and finite element spaces, $Ra = 10^9$, averaged over time. *th* indicates that $(\mathbb{Q}_2/\mathbb{Q}_1) \wedge \mathbb{Q}_1 \wedge (\mathbb{Q}_2/\mathbb{Q}_1)$ elements are used and $(\mathbb{Q}^+_2/\mathbb{Q}_1) \wedge \mathbb{Q}_1 \wedge (\mathbb{Q}^+_2/\mathbb{Q}_1)$ are denoted by *bb*. The label hu1 indicates that $\tau^{u/\theta}_{M/L} = \frac{1}{2}h/\|\boldsymbol{u}_h\|_{\infty,M/L}$. Nu^{ref} denotes DNS results from [21]

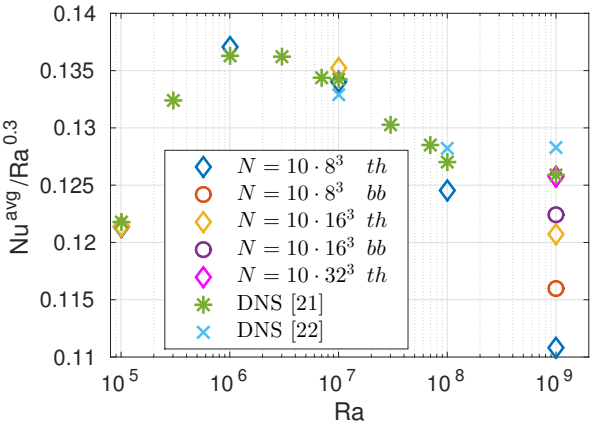

Fig. 4: $Nu/Ra^{0.3}$ ($\Gamma = 1$, $Pr = 0.786$) for an anisotropic grid with $N \in \{10 \cdot 8^3, 10 \cdot 16^3\}$ cells, compared with DNS data from [21] ($\Gamma = 1$, $Pr = 0.786$) and [22] ($\Gamma = 1$, $Pr = 0.7$). The grid is transformed via T_{xyz} for $N \in \{10 \cdot 8^3, 10 \cdot 16^3\}$ and via T_z for $N = 10 \cdot 32^3$. The label *th* indicates that $(\mathbb{Q}_2/\mathbb{Q}_1) \wedge \mathbb{Q}_1 \wedge (\mathbb{Q}_2/\mathbb{Q}_1)$ elements are used and $(\mathbb{Q}_2^+/\mathbb{Q}_1) \wedge \mathbb{Q}_1 \wedge (\mathbb{Q}_2^+/\mathbb{Q}_1)$ are denoted by *bb*. For $10^5 \leq Ra \leq 10^8$, $(\gamma_M, \tau_M^u, \tau_L^\theta) = (0.1, 0, 0)$ is chosen; $(\gamma_M, \tau_M^u, \tau_L^\theta) = (0.01, \frac{1}{2}h/\|\boldsymbol{u}_h\|_{\infty,M}, 0)$ in case of $Ra = 10^9$

Figure 4 provides an overview over the obtained results (using the respective optimal stabilization parameters and an anisotropic grid). We compare the reduced Nusselt numbers $Nu/Ra^{0.3}$ for different finite element spaces, indicated by *th* and *bb* as above, with DNS data from the literature. The Grossmann-Lohse theory from [23] suggests that there is a scaling law of the Nusselt number depending on Ra (at fixed Pr) that holds over wide parameter ranges. The reduced Nusselt number calculated in our experiments is nearly constant. However, one does not observe a global behavior of the Nusselt number as $Nu \propto Ra^{0.3}$. But as in [21], a smooth transition between different Ra-regimes $Ra \leq 10^6$, $10^6 \leq Ra \leq 10^8$ and $Ra \geq 10^8$ can be expected.

	$\langle \delta_\theta \rangle$			$\langle \delta_\theta \rangle \propto Ra^m$	
	$Ra = 10^5$	$Ra = 10^7$	$Ra = 10^9$	m	m^{ref}
top	0.1295	0.0311	0.0084	-0.2970	-0.285
bottom	0.1295	0.0293	0.0085	-0.2957	-0.285

Table 4: Thermal boundary layer thicknesses at the top and bottom plates $\langle \delta_\theta \rangle^{top/bottom}$, averaged over $r = \sqrt{x^2 + y^2} \in [0, \frac{1}{2}]$, and slopes $m^{top/bottom}$ resulting from the fitting $\langle \delta_\theta \rangle \propto Ra^m$. The grid with $N = 10 \cdot 16^3$ cells is transformed via T_{xyz}; $\mathbb{Q}_2 \wedge \mathbb{Q}_1 \wedge \mathbb{Q}_2$ elements are used. $\gamma_M = 0.1$ for $Ra \in \{10^5, 10^7\}$ and $\gamma_M = 0.01$ for $Ra = 10^9$. m^{ref} denotes the slope proposed by [21]

Table 4 validates that a grid transformed via T_{xyz} (together with grad-div stabilization) resolves the boundary layer: For a grid with $N = 10 \cdot 16^3$ cells, the dependence between Ra and the resulting thermal boundary layer thickness $\langle \delta_\theta \rangle$ is in good agreement with the law $\langle \delta_\theta \rangle \propto Ra^{-0.285}$ suggested by [21]. Here, the thermal boundary layer thickness δ_θ is calculated via the so-called slope criterion as in [21]. δ_θ is the distance from the boundary at which the linear approximation of temperature profile at the boundary crosses the line $\theta = 0$. $\langle \delta_\theta \rangle$ denotes the average over $r = \sqrt{x^2 + y^2} \in [0, \frac{1}{2}]$.

All in all, our simulations illustrate that we obtain surprisingly well approximated benchmark quantities even on relatively coarse meshes (compared with DNS from the reference data). For example, for the grid with $N = 10 \cdot 16^3$ cells, we have a total number of approximately $1,400,000$ degrees of freedom (DoFs) in case of $(\mathbb{Q}_2/\mathbb{Q}_1) \wedge \mathbb{Q}_1 \wedge (\mathbb{Q}_2/\mathbb{Q}_1)$ elements. Enriched $(\mathbb{Q}_2^+/\mathbb{Q}_1) \wedge \mathbb{Q}_1 \wedge (\mathbb{Q}_2^+/\mathbb{Q}_1)$ elements result in $1,900,000$ DoFs for $N = 10 \cdot 16^3$ cells. Refinement increases the number of DoFs roughly by a factor of 8. In comparison, the DNS in [21] requires approximately $1,500,000,000$ DoFs.

The key ingredients are grad-div stabilization and a grid that resolves the boundary layer. In case of isotropic grids, that are not adapted to the problem, LPS SU stabilization for the temperature becomes necessary. Bubble enrichment enhances the accuracy on all grids.

6 Summary and Conclusions

We considered conforming finite element approximations of the time-dependent Oberbeck-Boussinesq problem with inf-sup stable approximation of velocity and pressure. In order to handle spurious oscillations due to dominating convection or poor mass conservation of the numerical solution, we introduced a stabilization method that combines the idea of local projection stabilization with streamline upwinding and grad-div stabilization.

A stability and convergence analysis is provided for the arising nonlinear semi-discrete problem. We can show that the Gronwall constant does not depend on the kinetic and thermal diffusivities ν and α for velocities and temperatures satisfying $\boldsymbol{u} \in [L^\infty(0,T;W^{1,\infty}(\Omega))]^d$, $\boldsymbol{u}_h \in [L^\infty(0,T;L^\infty(\Omega))]^d$, $\theta \in L^\infty(0,T;W^{1,\infty}(\Omega))$. The approach relies on the existence of a (quasi-)local interpolation operator $j_u \colon \boldsymbol{V}^{div} \to \boldsymbol{V}_h^{div}$ preserving the divergence (see [15]). In contrast to the estimates in [7] and [8] for the Oseen and Navier-Stokes problem, we can circumvent a mesh width restriction of the form

$$Re_M := \frac{h_M \|\boldsymbol{u}_h\|_{\infty,M}}{\nu} \leq \frac{1}{\sqrt{\nu}} \quad \text{and} \quad Pe_L := \frac{h_L \|\boldsymbol{u}_h\|_{\infty,L}}{\alpha} \leq \frac{1}{\sqrt{\alpha}}$$

even if no compatibility condition between fine and coarse velocity and temperature spaces holds. Therefore, the analysis is valid for almost all inf-sup stable finite element settings.

Furthermore, we suggest a suitable parameter design depending on the coarse spaces $\boldsymbol{D}_M^u$ and $\boldsymbol{D}_L^\theta$. Note that a broad range of LPS SU parameters τ_M^u, τ_L^θ is possible. In particular, we achieve the same rate of convergence in the considered error norm if τ_M^u and τ_L^θ are set to zero. The LPS SU stabilization gives additional control over the velocity gradient in streamline direction.

It is indicated by our analysis and numerical experiments that $\gamma_M = \mathcal{O}(1)$ is essential for improved mass conservation and velocity estimates in $W^{1,2}(\Omega)$. We point out that grad-div stabilization proves essential for the independence of the Gronwall constant $C_G(\boldsymbol{u}, \theta, \boldsymbol{u}_h)$ from ν and α. Though the analysis assumes isotropic grids, the use of anisotropic ones in our numerical examples does not lead to any problems. The need for additional stabilization can be avoided if the grids are adapted to the problem. This is agreement with the numerical tests performed in [7]. Especially, for boundary layer flows, the SUPG-type stabilization $\tau_M^u \sim h/\|\boldsymbol{u}_h\|_{\infty,M}$ seems to be suited for modeling unresolved velocity scales if isotropic meshes are used. The combination with enriched elements is favorable.

For Rayleigh-Bénard convection, the combination of grad-div stabilization, a problem adjusted mesh and suitable ansatz spaces yields results that approximate DNS data.

7 Appendix

Lemma 1 *Let $\epsilon > 0$ and $(\boldsymbol{u}, p, \theta) \in \boldsymbol{V}^{div} \times Q \times \Theta$, $(\boldsymbol{u}_h, p_h, \theta_h) \in \boldsymbol{V}_h^{div} \times Q_h \times \Theta_h$ be solutions of (2)-(3) and (7)-(8) satisfying $\boldsymbol{u} \in [W^{1,\infty}(\Omega)]^d$, $\theta \in W^{1,\infty}(\Omega)$ and $\boldsymbol{u}_h \in [L^\infty(\Omega)]^d$. If Assumptions 1 and 2 hold, we can estimate the difference of the convective terms in the momentum equation*

$$
\begin{aligned}
&c_u(\boldsymbol{u}; \boldsymbol{u}, \boldsymbol{e}_{u,h}) - c_u(\boldsymbol{u}_h; \boldsymbol{u}_h, \boldsymbol{e}_{u,h}) \\
&\leq \frac{C}{\epsilon} \sum_{M \in \mathcal{M}_h} \frac{1}{h_M^2} \|\boldsymbol{\eta}_{u,h}\|_{0,M}^2 + 3\epsilon |||\boldsymbol{\eta}_{u,h}|||_{LPS}^2 + 3\epsilon |||\boldsymbol{e}_{u,h}|||_{LPS}^2 \\
&\quad + \Bigg[|\boldsymbol{u}|_{W^{1,\infty}(\Omega)} + \epsilon \max_{M \in \mathcal{M}_h} \{h_M^2 |\boldsymbol{u}|_{W^{1,\infty}(M)}^2\} + \frac{C}{\epsilon} \max_{M \in \mathcal{M}_h} \left\{ \frac{h_M^2}{\gamma_M} |\boldsymbol{u}|_{W^{1,\infty}(M)}^2 \right\} \\
&\qquad + \frac{C}{\epsilon} \max_{M \in \mathcal{M}_h} \{\gamma_M^{-1} \|\boldsymbol{u}\|_{\infty,M}^2\} + \epsilon \|\boldsymbol{u}_h\|_\infty^2 \Bigg] \|\boldsymbol{e}_{u,h}\|_0^2
\end{aligned}
$$

with C independent of h_M, h_L, ϵ, the problem parameters and the solutions. The difference of the convective terms in the Fourier equation can be bounded as

$$
\begin{aligned}
&c_\theta(\boldsymbol{u}; \theta, e_{\theta,h}) - c_\theta(\boldsymbol{u}_h; \theta_h, e_{\theta,h}) \\
&\leq \frac{C}{\epsilon} \sum_{M \in \mathcal{M}_h} h_M^{-2} \|\boldsymbol{\eta}_{u,h}\|_{0,M}^2 + 3\epsilon |||\boldsymbol{\eta}_{u,h}|||_{LPS}^2 + 3\epsilon |||\boldsymbol{e}_{u,h}|||_{LPS}^2 \\
&\quad + \frac{1}{2} |\theta|_{W^{1,\infty}(\Omega)} \|\boldsymbol{e}_{u,h}\|_0^2 + \frac{C}{\epsilon} \sum_{L \in \mathcal{L}_h} h_L^{-2} \|\eta_{\theta,h}\|_{0,L}^2 \\
&\quad + \|e_{\theta,h}\|_0^2 \Bigg(\frac{1}{2} |\theta|_{W^{1,\infty}(\Omega)} + \epsilon \|\boldsymbol{u}_h\|_\infty^2 + \epsilon \max_{M \in \mathcal{M}_h} \{h_M^2 |\theta|_{W^{1,\infty}(M)}^2\} \\
&\qquad\qquad + \frac{C}{\epsilon} \max_{M \in \mathcal{M}_h} \left\{ \frac{h_M^2}{\gamma_M} |\theta|_{W^{1,\infty}(M)}^2 \right\} + \frac{C}{\epsilon} \max_{M \in \mathcal{M}_h} \{\gamma_M^{-1} \|\theta\|_{\infty,M}^2\} \Bigg)
\end{aligned}
$$

with $C > 0$ independent of the problem parameters, h_M, h_L and the solutions.

Proof Similar estimates can be performed for velocity and temperature. We present the steps for the velocity; for details for the temperature terms, we refer the reader to [16].
We choose the same interpolation operators $j_u \colon \boldsymbol{V}^{div} \to \boldsymbol{V}_h^{div}$ and $j_\theta \colon \Theta \to \Theta_h$ as in Theorem 2. With the splitting $\boldsymbol{\eta}_{u,h} + \boldsymbol{e}_{u,h} = (\boldsymbol{u} - j_u\boldsymbol{u}) + (j_u\boldsymbol{u} - \boldsymbol{u}_h)$ from (13) and integration by parts, we have

$$\begin{aligned} &c_u(\boldsymbol{u};\boldsymbol{u},\boldsymbol{e}_{u,h}) - c_u(\boldsymbol{u}_h;\boldsymbol{u}_h,\boldsymbol{e}_{u,h}) \\ &= \underbrace{((\boldsymbol{u}-\boldsymbol{u}_h)\cdot\nabla\boldsymbol{u},\boldsymbol{e}_{u,h})}_{=:T_1^u} + \underbrace{(\boldsymbol{u}_h\cdot\nabla(\boldsymbol{u}-j_u\boldsymbol{u}),\boldsymbol{e}_{u,h})}_{=:T_2^u} - \frac{1}{2}\underbrace{((\nabla\cdot\boldsymbol{u}_h)j_u\boldsymbol{u},\boldsymbol{e}_{u,h})}_{=:T_3^u}. \end{aligned}$$

Now, we bound each term separately. Using Young's inequality with $\epsilon > 0$, we calculate:

$$\begin{aligned} T_1^u &\le \sum_{M\in\mathcal{M}_h} \|\nabla\boldsymbol{u}\|_{\infty,M}\Big(\|\boldsymbol{e}_{u,h}\|_{0,M}^2 + \|\boldsymbol{\eta}_{u,h}\|_{0,M}\|\boldsymbol{e}_{u,h}\|_{0,M}\Big) \\ &\le |\boldsymbol{u}|_{W^{1,\infty}(\Omega)}\|\boldsymbol{e}_{u,h}\|_0^2 + \sum_{M\in\mathcal{M}_h}\frac{1}{h_M}|\boldsymbol{u}|_{W^{1,\infty}(M)}\|\boldsymbol{\eta}_{u,h}\|_{0,M}h_M\|\boldsymbol{e}_{u,h}\|_{0,M} \qquad (34) \\ &\le \frac{1}{4\epsilon}\sum_{M\in\mathcal{M}_h}\frac{1}{h_M^2}\|\boldsymbol{\eta}_{u,h}\|_{0,M}^2 + \Big(|\boldsymbol{u}|_{W^{1,\infty}(\Omega)} + \epsilon\max_{M\in\mathcal{M}_h}\{h_M^2|\boldsymbol{u}|_{W^{1,\infty}(M)}^2\}\Big)\|\boldsymbol{e}_{u,h}\|_0^2. \end{aligned}$$

For the term T_2^u, we have via integration by parts

$$T_2^u = (\boldsymbol{u}_h\cdot\nabla\boldsymbol{\eta}_{u,h},\boldsymbol{e}_{u,h}) = -(\boldsymbol{u}_h\cdot\nabla\boldsymbol{e}_{u,h},\boldsymbol{\eta}_{u,h}) - ((\nabla\cdot\boldsymbol{u}_h)\boldsymbol{e}_{u,h},\boldsymbol{\eta}_{u,h}) =: T_{21}^u + T_{22}^u.$$

Term T_{21}^u is the most critical one. We calculate using Assumption 2 and Young's inequality:

$$\begin{aligned} T_{21}^u = -(\boldsymbol{u}_h\cdot\nabla\boldsymbol{e}_{u,h},\boldsymbol{\eta}_{u,h}) &\le \sum_{M\in\mathcal{M}_h}\|\boldsymbol{u}_h\|_{\infty,M}\|\nabla\boldsymbol{e}_{u,h}\|_{0,M}\|\boldsymbol{\eta}_{u,h}\|_{0,M} \\ &\le C\sum_{M\in\mathcal{M}_h}\|\boldsymbol{u}_h\|_{\infty,M}\|\boldsymbol{e}_{u,h}\|_{0,M}h_M^{-1}\|\boldsymbol{\eta}_{u,h}\|_{0,M} \qquad (35) \\ &\le \epsilon\|\boldsymbol{u}_h\|_\infty^2\|\boldsymbol{e}_{u,h}\|_0^2 + \frac{C}{\epsilon}\sum_{M\in\mathcal{M}_h}h_M^{-2}\|\boldsymbol{\eta}_{u,h}\|_{0,M}^2. \end{aligned}$$

Using $(\nabla\cdot\boldsymbol{u},q) = 0$ for all $q \in L^2(\Omega)$, Assumption 1 and Young's inequality with $\epsilon > 0$, we obtain

$$\begin{aligned} T_{22}^u = -((\nabla\cdot\boldsymbol{u}_h)\boldsymbol{\eta}_{u,h},\boldsymbol{e}_{u,h}) \ &= ((\nabla\cdot(\boldsymbol{\eta}_{u,h}+\boldsymbol{e}_{u,h}))\boldsymbol{\eta}_{u,h},\boldsymbol{e}_{u,h}) \\ &\le \sum_{M\in\mathcal{M}_h}\|\boldsymbol{\eta}_{u,h}\|_{\infty,M}\Big(\|\nabla\cdot\boldsymbol{e}_{u,h}\|_{0,M} + \|\nabla\cdot\boldsymbol{\eta}_{u,h}\|_{0,M}\Big)\|\boldsymbol{e}_{u,h}\|_{0,M} \qquad (36) \\ &\le \sum_{M\in\mathcal{M}_h}\frac{Ch_M}{\sqrt{\gamma_M}}|\boldsymbol{u}|_{W^{1,\infty}(M)}\sqrt{\gamma_M}\Big(\|\nabla\cdot\boldsymbol{e}_{u,h}\|_{0,M} + \|\nabla\cdot\boldsymbol{\eta}_{u,h}\|_{0,M}\Big)\|\boldsymbol{e}_{u,h}\|_{0,M} \\ &\le \epsilon|||\boldsymbol{\eta}_{u,h}|||_{LPS}^2 + \epsilon|||\boldsymbol{e}_{u,h}|||_{LPS}^2 + \frac{C}{\epsilon}\max_{M\in\mathcal{M}_h}\Big\{\frac{h_M^2}{\gamma_M}|\boldsymbol{u}|_{W^{1,\infty}(M)}^2\Big\}\|\boldsymbol{e}_{u,h}\|_0^2. \end{aligned}$$

Utilizing the splitting according to (13), we have

$$T_3^u = ((\nabla \cdot \boldsymbol{u}_h) j_u \boldsymbol{u}, \boldsymbol{e}_{u,h}) = -((\nabla \cdot \boldsymbol{u}_h)\boldsymbol{\eta}_{u,h}, \boldsymbol{e}_{u,h}) + ((\nabla \cdot \boldsymbol{u}_h)\boldsymbol{u}, \boldsymbol{e}_{u,h}) = T_{22}^u + T_{32}^u.$$

and use the same estimate as in (36). For the term T_{32}^u, we use that $(\nabla \cdot \boldsymbol{u}, q) = 0$ for all $q \in L^2(\Omega)$ and Young's inequality:

$$\begin{aligned}
|T_{32}^u| &= |(\nabla \cdot \boldsymbol{u}_h, \boldsymbol{u} \cdot \boldsymbol{e}_{u,h})| = |(\nabla \cdot (-\boldsymbol{\eta}_{u,h} - \boldsymbol{e}_{u,h} + \boldsymbol{u}), \boldsymbol{u} \cdot \boldsymbol{e}_{u,h})| \\
&\leq |(\nabla \cdot \boldsymbol{\eta}_{u,h}, \boldsymbol{u} \cdot \boldsymbol{e}_{u,h})| + |(\nabla \cdot \boldsymbol{e}_{u,h}, \boldsymbol{u} \cdot \boldsymbol{e}_{u,h})| \\
&\leq \sum_{M \in \mathcal{M}_h} \Big(\|\boldsymbol{u}\|_{\infty,M} \sqrt{\gamma_M} \|\nabla \cdot \boldsymbol{\eta}_{u,h}\|_{0,M} \frac{1}{\sqrt{\gamma_M}} \|\boldsymbol{e}_{u,h}\|_{0,M} \\
&\qquad + \|\boldsymbol{u}\|_{\infty,M} \sqrt{\gamma_M} \|\nabla \cdot \boldsymbol{e}_{u,h}\|_{0,M} \frac{1}{\sqrt{\gamma_M}} \|\boldsymbol{e}_{u,h}\|_{0,M} \Big) \\
&\leq \epsilon |||\boldsymbol{\eta}_{u,h}|||_{LPS}^2 + \epsilon |||\boldsymbol{e}_{u,h}|||_{LPS}^2 + \frac{C}{\epsilon} \max_{M \in \mathcal{M}_h} \{\gamma_M^{-1} \|\boldsymbol{u}\|_{\infty,M}^2\} \|\boldsymbol{e}_{u,h}\|_0^2.
\end{aligned} \tag{37}$$

Combining the above bounds (34)-(37) yields the claim.

References

1. J. Boussinesq, *Théorie analytique de la chaleur: mise en harmonie avec la thermodynamique et avec la théorie mécanique de la lumière*, vol. 2. Gauthier-Villars, 1903.
2. A. Oberbeck, "Über die Wärmeleitung der Flüssigkeiten bei Berücksichtigung der Strömungen infolge von Temperaturdifferenzen," *Annalen der Physik*, vol. 243, no. 6, pp. 271–292, 1879.
3. T. Gelhard, G. Lube, M. Olshanskii, and J.-H. Starcke, "Stabilized finite element schemes with LBB-stable elements for incompressible flows," *Journal of Computational and Applied Mathematics*, vol. 177, no. 2, pp. 243–267, 2005.
4. M. Case, V. Ervin, A. Linke, and L. Rebholz, "A connection between Scott-Vogelius and grad-div stabilized Taylor-Hood FE approximations of the Navier-Stokes equations," *SIAM Journal on Numerical Analysis*, vol. 49, no. 4, pp. 1461–1481, 2011.
5. G. Matthies, P. Skrzypacz, and L. Tobiska, "A unified convergence analysis for local projection stabilisations applied to the Oseen problem," *ESAIM-Mathematical Modelling and Numerical Analysis*, vol. 41, no. 4, pp. 713–742, 2007.
6. G. Matthies and L. Tobiska, "Local projection type stabilization applied to inf-sup stable discretizations of the Oseen problem," *IMA Journal of Numerical Analysis*, 2014.
7. H. Dallmann, D. Arndt, and G. Lube, "Local projection stabilization for the Oseen problem," *IMA Journal of Numerical Analysis*, 2015.
8. D. Arndt, H. Dallmann, and G. Lube, "Local projection FEM stabilization for the time-dependent incompressible Navier–Stokes problem," *Numerical Methods for Partial Differential Equations*, vol. 31, no. 4, pp. 1224–1250, 2015.
9. J. de Frutos, B. García-Archilla, V. John, and J. Novo, "Grad-div stabilization for the evolutionary Oseen problem with inf-sup stable finite elements," *Journal of Scientific Computing*, pp. 1–34, 2015.
10. J. Boland and W. Layton, "An analysis of the finite element method for natural convection problems," *Numerical Methods for Partial Differential Equations*, vol. 6, no. 2, pp. 115–126, 1990.
11. J. Boland and W. Layton, "Error analysis for finite element methods for steady natural convection problems," *Numerical functional analysis and optimization*, vol. 11, no. 5-6, pp. 449–483, 1990.
12. O. Dorok, W. Grambow, and L. Tobiska, *Aspects of finite element discretizations for solving the Boussinesq approximation of the Navier-Stokes equations*. Springer, 1994.
13. R. Codina, J. Principe, and M. Ávila, "Finite element approximation of turbulent thermally coupled incompressible flows with numerical sub-grid scale modelling," *International Journal of Numerical Methods for Heat & Fluid Flow*, vol. 20, no. 5, pp. 492–516, 2010.

14. J. Loewe and G. Lube, "A projection-based variational multiscale method for large-eddy simulation with application to non-isothermal free convection problems," *Mathematical Models and Methods in Applied Sciences*, vol. 22, no. 02, 2012.
15. V. Girault and L. Scott, "A quasi-local interpolation operator preserving the discrete divergence," *Calcolo*, vol. 40, no. 1, pp. 1–19, 2003.
16. H. Dallmann, *Finite Element Methods with Local Projection Stabilization for Thermally Coupled Incompressible Flow*. PhD thesis, University of Göttingen, 2015.
17. E. Jenkins, V. John, A. Linke, and L. Rebholz, "On the parameter choice in grad-div stabilization for incompressible flow problems," *Advances in Computational Mathematics*, 2013.
18. L. Timmermans, P. Minev, and F. Van De Vosse, "An approximate projection scheme for incompressible flow using spectral elements," *International journal for numerical methods in fluids*, vol. 22, no. 7, pp. 673–688, 1996.
19. J.-L. Guermond and J. Shen, "On the error estimates for the rotational pressure-correction projection methods," *Mathematics of Computation*, vol. 73, no. 248, pp. 1719–1737, 2004.
20. D. Arndt and H. Dallmann, "Error estimates for the fully discretized incompressible Navier-Stokes problem with LPS stabilization," tech. rep., Institute of Numerical and Applied Mathematics, Georg-August-University of Göttingen, 2015.
21. S. Wagner, O. Shishkina, and C. Wagner, "Boundary layers and wind in cylindrical Rayleigh–Bénard cells," *Journal of Fluid Mechanics*, vol. 697, pp. 336–366, 2012.
22. J. Bailon-Cuba, M. Emran, and J. Schumacher, "Aspect ratio dependence of heat transfer and large-scale flow in turbulent convection," *Journal of Fluid Mechanics*, vol. 655, pp. 152–173, 2010.
23. S. Grossmann and D. Lohse, "Scaling in thermal convection: a unifying theory," *Journal of Fluid Mechanics*, vol. 407, pp. 27–56, 2000.